A^2RC: An Accurate Array Response Control Algorithm for Pattern Synthesis

Xuejing Zhang, *Student Member, IEEE*, Zishu He, *Member, IEEE*, Bin Liao, *Senior Member, IEEE*, Xuepan Zhang, Ziyang Cheng, and Yanxi Lu, *Student Member, IEEE*

***Abstract*—This paper presents a novel accurate array response control algorithm, abbreviated as A^2RC, and its application to array pattern synthesis. The proposed A^2RC algorithm deals with the problem of how to accurately control the array response at a given direction. Starting from the adaptive array theory, a deep analysis of the optimal weight vector is carried out. It is found that the normalized response at a given direction can be accurately adjusted to an arbitrary level, by means of making some simple modification to the initial weight vector. On this basis, all possible weight vectors, which have a specific form and can make the normalized response at the given direction equal to the prescribed value, are first figured out. Then, an effective approach to selecting the most appropriate one, which would cause the least pattern distortion, is devised. By applying the A^2RC algorithm, a new pattern synthesis approach for arbitrary arrays is developed. In this approach, the array pattern is adjusted in a point-by-point manner by successively modifying the weight vector. Contrary to the conventional approaches that assign artificial interferences in an *ad hoc* way, our approach is able to obtain the weight vector without iteratively determining the powers of the artificial interferences. Extensive simulation results are provided to demonstrate the performance of the A^2RC algorithm in array response control and the effectiveness of this algorithm in pattern synthesis under various situations.**

***Index Terms*—Array response control, array pattern synthesis, adaptive array theory, array signal processing.**

I. Introduction

PATTERN synthesis is one of the fundamental problems in array signal processing. It has been extensively investigated over the last several decades owing to its vast applications such as radar, remote sensing and wireless communications [1]–[4]. In brief, pattern synthesis is to design a specific pattern by determining appropriate weights of the array elements. For example, in radar systems, it is desired to design a pattern with low sidelobe levels to suppress the noise and interference. In communication systems, controlling the array beam pattern to form nulls at the directions of jammings has become a common anti-interference measure. Additionally, in remote sensing applications, producing a pattern with a broad mainlobe is required to achieve a wide coverage area.

Quite a number of pattern synthesis approaches have been proposed in the literature. In [5], Dolph provided an elegant solution to the problem of obtaining a Chebyshev pattern, which yields a minimum uniform sidelobe level for a given mainlobe width. It should be noticed that this method is limited to uniform linear arrays (ULAs) in general. As a result, many efforts have been devoted to pattern synthesis when the array elements are not equally spaced and/or the elements have nonisotropic patterns [6]–[8]. Among them, a noteworthy stream is the utilization of global search. One of the most popular strategies is the so-called genetic algorithm, which performs the genetic operations in order to obtain the optimum solution [6]. Other common global search algorithms applied to pattern synthesis include particle swarm optimization [7] and simulated annealing [8]. It is known that a main shortcoming of these approaches is the prohibitive amount of computation time, which significantly limits the practical use.

For arbitrary arrays, many algorithms to achieve desired patterns have been proposed by taking advantage of the adaptive array theory [9]–[11]. For instance, the simple approach in [12] involves the procedure of solving a sequence of linearly constrained least squares problems. In [13], Olen and Compton developed a systematic approach by assigning artificial interferers in sidelobe regions. The power levels of interferers at different sidelobes are iteratively adjusted according to the deviation from the current synthesized pattern to the desired one. This algorithm is able to control the sidelobe levels effectively, but is lack of ability to control the responses in mainlobe region. More importantly, this method needs to determine the mainlobe region at each iteration and it suffers from high computational complexity. Thus, attempts have been made to overcome these shortcomings. To reduce the computational complexity and improve the flexibility, an iterative method was developed in [14] to shape the array pattern. This method stems from [13] and is able to control the responses in both sidelobe region and mainlobe region. Another modification to [13] which aims at improving the convergence rate and computational efficiency was studied in [15], [16]. It is worth noting that in the above-mentioned methods, some parameters, such as the power levels of artificial interferences, are selected in an *ad hoc* way.

Manuscript received July 19, 2016; accepted December 26, 2016. Date of publication January 9, 2017; date of current version January 30, 2017. The associate editor coordinating the review of this manuscript and approving it for publication was Dr. Pengfei Xia. This work was supported by the National Nature Science Foundation of China under Grant 61671139 and Grant 61401284.

X. Zhang, Z. He, Z. Cheng, and Y. Lu are with the University of Electronic Science and Technology of China, Chengdu 611731, China (e-mail: xjzhang7@163.com; zshe@uestc.edu.cn; zeeyoungcheng@163.com; Yanxi.Lu@outlook.com).

B. Liao is with the College of Information Engineering, Shenzhen University, Shenzhen 518060, China (e-mail: binliao@szu.edu.cn).

X. Zhang is with the Qian Xuesen Laboratory of Space Technology, Beijing 100094, China (e-mail: zhangxuepan@qxslab.cn).

Color versions of one or more of the figures in this paper are available online at http://ieeexplore.ieee.org.

Digital Object Identifier 10.1109/TSP.2017.2649487

Owing to the development of optimization techniques, pattern synthesis has attracted much interest in the past several years. In [17], the problem of pattern synthesis is modeled to be a convex optimization problem which can be efficiently solved by interior-point methods. For robust array pattern synthesis, second-order cone programming and semidefinite programming have been employed in [18]. The semidefinite relaxation is utilized for designing various patterns in [19]. For a more complete review of pattern synthesis, the interested reader is referred to the recent work [20].

It should be noticed that in general the aforementioned methods cannot flexibly control the array response. The weight vector has to be completely redesigned even if only a slight change of the desired pattern is needed. This motivates us to develop a novel accurate array response control (A^{2}RC) algorithm, which considers the problem of how to accurately control the array response at a given direction. To this end, a deep analysis of the optimal weight vector is carried out to show that the normalized response at a fixed direction can be accurately adjusted to an arbitrary level by making some simple modification to the initial weight vector. On this basis, the problem of how to make the normalized level at a given direction equal to a prescribed value is formulated. In addition, an effective approach to selecting an appropriate solution is developed by minimizing the pattern distortion. According to the A^{2}RC algorithm, we make the normalized response of a direction equal to the desired level point-by-point, and succeed to synthesize patterns for arbitrary arrays, including arrays with nonisotropic elements and two-dimensional (2-D) arrays. Comparing with the traditional methods which were also based on the theory of adaptive array [12]–[16], the proposed A^{2}RC based pattern synthesis approach is capable of accurately and flexibly controlling the array response level, and has great application value due to its simplicity and effectiveness.

The paper is organized as follows. In Section II, the problem formulation of pattern synthesis and preliminary adaptive array theory are given. The proposed A^{2}RC algorithm is analyzed in Section III and its application to pattern synthesis is discussed in Section IV. In Section V, extensive numerical examples are conducted to demonstrate the excellent performance of the proposed method. Conclusions are drawn in Section VI.

II. Problem Statement and Adaptive Array Theory

A. Pattern Synthesis Formulation

Let us consider an N-element array in arbitrary geometry. Without loss of generality and for the sake of clarity, we focus on herein the problem of one-dimensional pattern synthesis. The steering vector in direction θ can be written as

$$\mathbf{a}(\theta) = [g_1(\theta)e^{-j\omega\tau_1(\theta)}, \ldots, g_N(\theta)e^{-j\omega\tau_N(\theta)}]^{\mathrm{T}} \tag{1}$$

where $(\cdot)^{\mathrm{T}}$ denotes the transpose operator, $j = \sqrt{-1}$ is the imaginary unit, $g_n(\theta)$ $(n = 1, \ldots, N)$ denotes the pattern of the nth element, $\tau_n(\theta)$ represents the time-delay between the nth element and the reference point, ω denotes the operating frequency. The array response then can be expressed as

$$f(\theta) = \mathbf{w}^{\mathrm{H}}\mathbf{a}(\theta) \tag{2}$$

where $(\cdot)^{\mathrm{H}}$ denotes the conjugate transpose, $\mathbf{w}$ is the weight vector. The problem of pattern synthesis can be stated as: finding an appropriate weight vector that makes the amplitude response $|f(\theta)|$ meeting some specific requirements.

B. Adaptive Array Theory

It can be seen that the above pattern synthesis formulation is data-independent. According to the adaptive array theory, the beampattern can be adaptively synthesized with the data received. In this case, the weight vector $\mathbf{w}$ is called adaptive beamformer, which can be optimally obtained by maximizing the output signal-to-interference-plus-noise ratio (SINR). More precisely, the output of the beamformer is described as $y(t) = \mathbf{w}^{\mathrm{H}}\mathbf{x}(t)$, where $\mathbf{x}(t)$ is the $N \times 1$ complex snapshot vector of the array observation which is composed of the components of signal, interference and noise. It is known that the optimal weight vector $\mathbf{w}_{opt}$, which maximizes the SINR, is given by

$$\mathbf{w}_{opt} = \alpha\mathbf{R}_{n+i}^{-1}\mathbf{a}(\theta_0) \tag{3}$$

where α is the normalization factor that does not affect the output SINR, $\mathbf{a}(\theta_0)$ is the signal steering vector, $\mathbf{R}_{n+i}$ denotes the $N \times N$ noise-plus-interference covariance matrix. When considering a single interference, we can express $\mathbf{R}_{n+i}$ as

$$\mathbf{R}_{n+i} = \sigma_n^2\mathbf{I} + \sigma_i^2\mathbf{a}(\theta_i)\mathbf{a}^{\mathrm{H}}(\theta_i) \tag{4}$$

provided that the noise is spatially-white and independent of the interference signal. In (4), $\mathbf{I}$ is the identity matrix, σ_n^2 and σ_i^2 stand for noise and interference powers, respectively, and $\mathbf{a}(\theta_i)$ is the interference steering vector. The pattern synthesized by the optimal weight vector $\mathbf{w}_{opt}$ is capable of forming a deep null in the direction of interference. This property will be exploited to develop the novel A^{2}RC algorithm in what follows.

III. The Proposed A^{2}RC Algorithm

Although the data-dependent adaptive beamforming approaches are able to synthesize array patterns with deep nulls at the interference directions, from the perspective of data-independent pattern synthesis, the problem of how to accurately control the array response as desired at a specific direction or region has not been adequately addressed. This motivates us to introduce a novel A^{2}RC algorithm in this section. First, the optimal weight vector is analyzed and a novel strategy to adjust the response level is proposed. Then, the problem of determining the vector is formulated and the corresponding solution is derived analytically. Finally, a simple and effective approach to achieving desired pattern is devised.

A. Weight Vector Analysis

Applying the matrix inversion lemma, the optimal array weight vector (3) can be rewritten as

$$\begin{aligned}\mathbf{w_{opt}} &= \alpha\mathbf{R}_{n+i}^{-1}\mathbf{a}(\theta_0) \\ &= \frac{\alpha}{\sigma_n^2}\left(\mathbf{a}(\theta_0) - \frac{\frac{\sigma_i^2}{\sigma_n^2}\mathbf{a}(\theta_i)\mathbf{a}^{\mathrm{H}}(\theta_i)\mathbf{a}(\theta_0)}{1 + \frac{\sigma_i^2}{\sigma_n^2}\|\mathbf{a}(\theta_i)\|_2^2}\right)\end{aligned} \tag{5}$$

where $\|\cdot\|_2$ gives the Euclidean norm of a vector, the common factor α/σ_n^2 does not affect the ultimate performance and will

be omitted in the interest of brevity. Thus, the optimal weight vector is alternatively expressed as

$$\mathbf{w}_\star = \mathbf{w}_0 + \mu\mathbf{a}(\theta_i) \tag{6}$$

where $\mathbf{w}_0$ is defined as

$$\mathbf{w}_0 \triangleq \mathbf{a}(\theta_0) \tag{7}$$

which can be regarded as a quiescent weight or initial weight, and μ is a complex number given by

$$\mu = -\frac{\text{INR}\mathbf{a}^{\text{H}}(\theta_i)\mathbf{a}(\theta_0)}{1+\text{INR}\|\mathbf{a}(\theta_i)\|_2^2} \tag{8}$$

where

$$\text{INR} = \sigma_i^2/\sigma_n^2 \tag{9}$$

denotes the interference-to-noise ratio.

From (6), it is seen that the optimal weight vector can be interpreted as a sum of two terms. The first term $\mathbf{w}_0$ is the so-called quiescent weight that has no ability to null interference. To be consistent with the following analysis, we prefer to name $\mathbf{w}_0$ as initial weight, since $\mathbf{w}_\star$ is achieved by making some modification to $\mathbf{w}_0$. The second term $\mu\mathbf{a}(\theta_i)$ is the interference steering vector multiplied by a complex factor μ, which is a function of INR. As a result, the power response $P_\star(\theta)$ can be written as

$$\begin{aligned} P_\star(\theta) = |\mathbf{w}_\star^{\text{H}}\mathbf{a}(\theta)|^2 &= |\mathbf{w}_0^{\text{H}}\mathbf{a}(\theta)|^2 + |\mu^* v(\theta,\theta_i)|^2 \\ &\quad + 2\text{Re}(\mu\mathbf{w}_0^{\text{H}}\mathbf{a}(\theta)v(\theta_i,\theta)) \\ &= P_i(\theta) + P_a(\theta) + P_c(\theta) \end{aligned} \tag{10}$$

where $(\cdot)^*$ stands for the conjugate operator, $v(\theta_i,\theta)$ is the inner product of $\mathbf{a}(\theta_i)$ and $\mathbf{a}(\theta)$, i.e.,

$$v(\theta_i,\theta) = \mathbf{a}^{\text{H}}(\theta)\mathbf{a}(\theta_i) \tag{11}$$

and $P_i(\theta) \triangleq |\mathbf{w}_0^{\text{H}}\mathbf{a}(\theta)|^2$ represents the array power response corresponding to the initial weight vector $\mathbf{w}_0$, $P_a(\theta) \triangleq |\mu^* v(\theta,\theta_i)|^2$ is an non-negative additive term, and $P_c(\theta) \triangleq 2\text{Re}(\mu\mathbf{w}_0^{\text{H}}\mathbf{a}(\theta)v(\theta_i,\theta))$ is a cross term which could be either positive or negative.

To proceed, we define the normalized power response at θ_i with respect to the response at θ_0 for a given weight vector $\mathbf{w}$ as

$$L(\theta_i,\theta_0) = \frac{P(\theta_i)}{P(\theta_0)} = \frac{|\mathbf{w}^{\text{H}}\mathbf{a}(\theta_i)|^2}{|\mathbf{w}^{\text{H}}\mathbf{a}(\theta_0)|^2}. \tag{12}$$

Meanwhile, we name the denominator term of $L(\theta_i,\theta_0)$ as the normalized factor of normalized power response for ease of exposition.

As a result, for the initial weight vector $\mathbf{w}_0$, the normalized power response can be expressed as

$$L_0(\theta_i,\theta_0) = \frac{P_i(\theta_i)}{P_i(\theta_0)} = \frac{|\mathbf{w}_0^{\text{H}}\mathbf{a}(\theta_i)|^2}{|\mathbf{w}_0^{\text{H}}\mathbf{a}(\theta_0)|^2} = \frac{|v(\theta_i,\theta_0)|^2}{\|\mathbf{a}(\theta_0)\|_2^4} \tag{13}$$

and, for the optimal weight vector $\mathbf{w}_\star$, one gets

$$L_\star(\theta_i,\theta_0) = \frac{P_\star(\theta_i)}{P_\star(\theta_0)} = \frac{|\mathbf{w}_\star^{\text{H}}\mathbf{a}(\theta_i)|^2}{|\mathbf{w}_\star^{\text{H}}\mathbf{a}(\theta_0)|^2}. \tag{14}$$

Obviously, we have $L_\star(\theta_0,\theta_0) = L_0(\theta_0,\theta_0) = 1$.

It can be noticed that if the array weight vector is tuned from $\mathbf{w}_0$ to $\mathbf{w}_\star$ by adding a term $\mu\mathbf{a}(\theta_i)$, the normalized array response at a certain direction θ_i can be modified as well. This implies that by comparing the normalized power responses $L_0(\theta_i,\theta_0)$ and $L_\star(\theta_i,\theta_0)$, it is possible to find out the mechanism to accurately control the array response by modifying the weight vector. To this end, we first expand $L_\star(\theta_i,\theta_0)$ to the equation (15) at the bottom of this page. A careful examination of (13) and (15) illustrates if $\left|(\|\mathbf{a}(\theta_0)\|_2^2\cdot\|\mathbf{a}(\theta_i)\|_2^2 - |v(\theta_i,\theta_0)|^2)\text{INR} + \|\mathbf{a}(\theta_0)\|_2^2\right| < \|\mathbf{a}(\theta_0)\|_2^2$, then $L_\star(\theta_i,\theta_0) > L_0(\theta_i,\theta_0)$, and vice versa. Moreover, according to the Cauchy-Schwarz (C-S) inequality, we have $\|\mathbf{a}(\theta_0)\|_2^2\cdot\|\mathbf{a}(\theta_i)\|_2^2 \geq |v(\theta_i,\theta_0)|^2$. As a consequence, if we treat INR as a real-valued variable which can be both negative and positive, the following essential conclusion can be obtained:

$$L_\star(\theta_i,\theta_0)\begin{cases} > L_0(\theta_i,\theta_0), & \text{if INR} \in \mathbb{I} \\ \leq L_0(\theta_i,\theta_0), & \text{otherwise} \end{cases} \tag{16}$$

where $\mathbb{I} = \left(\frac{-2\|\mathbf{a}(\theta_0)\|_2^2}{\|\mathbf{a}(\theta_0)\|_2^2\|\mathbf{a}(\theta_i)\|_2^2 - |v(\theta_i,\theta_0)|^2}, 0\right)$.

It is noteworthy that from now on INR denotes a real-valued number only, whereas in the data-dependent processing algorithm it has to be non-negative. Therefore, in the sequel, we express $L_\star(\theta_i,\theta_0)$ as $L_\star(\theta_i,\theta_0,\text{INR})$. Obviously, it is readily verified that if $\text{INR} = 0$ or $\frac{-2\|\mathbf{a}(\theta_0)\|_2^2}{\|\mathbf{a}(\theta_0)\|_2^2\|\mathbf{a}(\theta_i)\|_2^2 - |v(\theta_i,\theta_0)|^2}$, we have $L_\star(\theta_i,\theta_0,\text{INR}) = L_0(\theta_i,\theta_0)$. To make the above points clearer, let us consider a ULA of $N = 16$ elements spaced by half wavelength, the curves of $L_\star(\theta_i,\theta_0,\text{INR})$ and $L_0(\theta_i,\theta_0)$ versus the INR for $\theta_0 = 0^\circ$ and $\theta_i = 20^\circ$ are plotted in Fig. 1. It is noticed that $L_\star(20^\circ,0^\circ,\text{INR})$ is less than $L_0(20^\circ,0^\circ)$ as long as $\text{INR} > 0$. As a matter of fact, this coincides with the data-dependent beamforming methods in which a null is formed at the interference direction, whereas the fixed beamformer $\mathbf{w}_0 = \mathbf{a}(\theta_0)$ does not. Another important observation is that for a given $\rho > 0$, there must exists (one or more) INR such that

$$\begin{aligned} L_\star(\theta_i,\theta_0) = \frac{|\mathbf{w}_\star^{\text{H}}\mathbf{a}(\theta_i)|^2}{|\mathbf{w}_\star^{\text{H}}\mathbf{a}(\theta_0)|^2} = \frac{P_i(\theta_i)+P_a(\theta_i)+P_c(\theta_i)}{P_i(\theta_0)+P_a(\theta_0)+P_c(\theta_0)} &= \frac{|v(\theta_i,\theta_0)|^2\left(1+\left(\frac{\sigma_i^2\|\mathbf{a}(\theta_i)\|_2^2}{\sigma_n^2+\sigma_i^2\|\mathbf{a}(\theta_i)\|_2^2}\right)^2 - \frac{2\sigma_i^2\|\mathbf{a}(\theta_i)\|_2^2}{\sigma_n^2+\sigma_i^2\|\mathbf{a}(\theta_i)\|_2^2}\right)}{\|\mathbf{a}(\theta_0)\|_2^4 + \left(\frac{\sigma_i^2|v(\theta_i,\theta_0)|^2}{\sigma_n^2+\sigma_i^2\|\mathbf{a}(\theta_i)\|_2^2}\right)^2 - \frac{2\sigma_i^2\|\mathbf{a}(\theta_0)\|_2^2|v(\theta_i,\theta_0)|^2}{\sigma_n^2+\sigma_i^2\|\mathbf{a}(\theta_i)\|_2^2}} \\ &= \frac{|v(\theta_i,\theta_0)|^2}{\left((\|\mathbf{a}(\theta_0)\|_2^2\cdot\|\mathbf{a}(\theta_i)\|_2^2 - |v(\theta_i,\theta_0)|^2)\text{INR} + \|\mathbf{a}(\theta_0)\|_2^2\right)^2} \end{aligned} \tag{15}$$

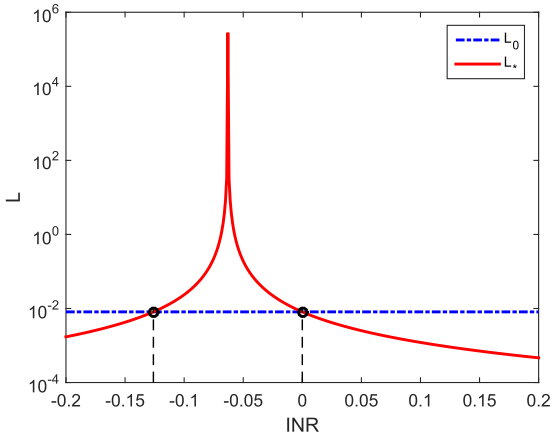

Fig. 1. Curves of $L_\star$ and L_0 versus INR for a ULA.

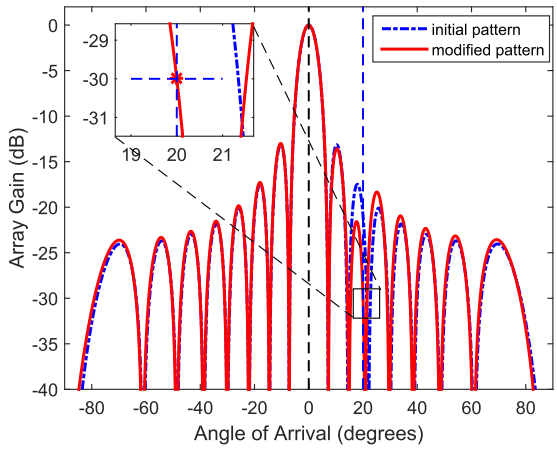

Fig. 2. Adjust $L_\star(20^\circ, 0^\circ)$ to -30 dB.

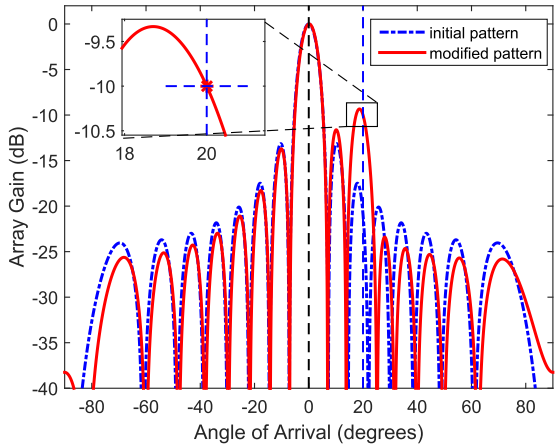

Fig. 3. Adjust $L_\star(20^\circ, 0^\circ)$ to -10 dB.

$L_\star(20^\circ, 0^\circ, \mathrm{INR}) = \rho$ if $\mathbf{a}(\theta_0) \neq \beta\mathbf{a}(\theta_i)$, where $\beta \in \mathbb{C}$. This leads to the following lemma.

Lemma 1: For any given θ_0 and θ_i satisfying $\forall\beta \in \mathbb{C}$, $\mathbf{a}(\theta_0) \neq \beta\mathbf{a}(\theta_i)$, then for $\forall\rho_\triangleright > 0$, there must exist $\mathrm{INR}_\triangleright \in \mathbb{R}$ such that $L_\star(\theta_i, \theta_0, \mathrm{INR}_\triangleright) = \rho_\triangleright$.

Proof: Given θ_0 and θ_i, if $\mathbf{a}(\theta_0) \neq \beta\mathbf{a}(\theta_i)$ for $\forall\beta$, we have $\|\mathbf{a}(\theta_0)\|_2^2\|\mathbf{a}(\theta_i)\|_2^2 > |v(\theta_i, \theta_0)|^2$ according to C-S inequality. Moreover, it is seen that $L_\star(\theta_i, \theta_0, \mathrm{INR}) \to 0$ as $\mathrm{INR} \to \pm\infty$, and $L_\star(\theta_i, \theta_0, \mathrm{INR}) \to +\infty$ when $\mathrm{INR} = \frac{-\|\mathbf{a}(\theta_0)\|_2^2}{\|\mathbf{a}(\theta_0)\|_2^2\|\mathbf{a}(\theta_i)\|_2^2 - |v(\theta_i,\theta_0)|^2}$. Due to the continuity of $L_\star(\theta_i, \theta_0, \mathrm{INR})$, we can conclude that for $\forall\rho_\triangleright > 0$, there must exist $\mathrm{INR}_\triangleright \in \mathbb{R}$ such that $L_\star(\theta_i, \theta_0, \mathrm{INR}_\triangleright) = \rho_\triangleright$. ■

Furthermore, as shown by (8), it is known that μ can be regarded as a function of INR. Thus, the following conclusion can be straightforwardly achieved.

Lemma 2: For any given θ_0 and θ_i satisfying $\forall\beta \in \mathbb{C}$, $\mathbf{a}(\theta_0) \neq \beta\mathbf{a}(\theta_i)$, then for $\forall\rho_\triangleright > 0$, there must exist $\mu_\triangleright \in \mathbb{C}$ and $\mathbf{w}_\triangleright = \mathbf{w}_0 + \mu_\triangleright\mathbf{a}(\theta_i)$ such that $L_\star(\theta_i, \theta_0) = \rho_\triangleright$.

Proof: Lemma 2 is a direct consequence of Lemma 1 and equation (8), the detailed proof is omitted. ■

From Lemma 2, it is observed that one may control the normalized power response at θ_i by adjusting the parameter μ. To illustrate the rationality of this result, we show in Figs. 2 and 3 that different μ can lead to different responses at a given θ. Again, in this example, a ULA with 16 isotropic sensors is considered, $\theta_i = 20^\circ$ and $\theta_0 = 0^\circ$. Figs. 2 and 3 show the synthesized patterns for different μ. More exactly, we take μ as $0.0119 + j0.0573$ and $-0.2974 + j0.0794$, and find that the corresponding responses at 20° are -30 dB and -10 dB, respectively.

Now, a quite natural question that one may raise is how to determine the value of μ to achieve the desired response at a specific direction. In the following subsections, this problem is discussed in detail.

B. Weight Vector Determination via EVD

In the last subsection, it has been shown that if we treat $\mathbf{a}(\theta_0)$ as an initial weight vector, a specific response at a given direction θ_i can be obtained by tuning the complex constant μ. This provides us useful insights to control the power response at a specific direction θ_i. To be specific, if we need to make the normalized power response at θ_1 equal to a specific value ρ_1, then, according to Lemma 2, there must exists a $\mu_1 \in \mathbb{C}$ and a corresponding weight vector $\mathbf{w}_1$ satisfying

$$\mathbf{w}_1 = \mathbf{w}_0 + \mu_1\mathbf{a}(\theta_1). \tag{17}$$

Since $\mathbf{w}_0$ and $\mathbf{a}(\theta_1)$ are known, the remaining task is to find an appropriate μ_1 to fulfill the response requirement. Assuming μ_1 has been obtained, if we need to control the response at another direction θ_2 to ρ_2, the weight vector is then adjusted to $\mathbf{w}_2 = \mathbf{w}_1 + \mu_2\mathbf{a}(\theta_2)$ with an appropriate μ_2. In such a manner, at the kth step, we need to find an appropriate $\mathbf{w}_k$ which makes the normalized power response at θ_k exactly equal to ρ_k. Given $\mathbf{w}_{k-1}$ obtained at the $(k-1)$th step, $\mathbf{w}_k$ can thus be expressed as

$$\mathbf{w}_k = \mathbf{w}_{k-1} + \mu_k\mathbf{a}(\theta_k). \tag{18}$$

It can be seen that it is possible to control the array response at a given direction by modifying the weight vector available rather than completely redesigning the weight vector.

Now, we discuss the approach to determining the parameter μ_k in each step. From (18), the normalized power response at θ_k can be described as

$$L_\star^{(k)}(\theta_k,\theta_0) = \frac{(\mathbf{w}_{k-1}+\mu_k\mathbf{a}(\theta_k))^{\mathrm{H}}\,\mathbf{a}(\theta_k)\mathbf{a}^{\mathrm{H}}(\theta_k)\,(\mathbf{w}_{k-1}+\mu_k\mathbf{a}(\theta_k))}{(\mathbf{w}_{k-1}+\mu_k\mathbf{a}(\theta_k))^{\mathrm{H}}\,\mathbf{a}(\theta_0)\mathbf{a}^{\mathrm{H}}(\theta_0)\,(\mathbf{w}_{k-1}+\mu_k\mathbf{a}(\theta_k))}. \tag{19}$$

Since the normalized power response at θ_k is ρ_k, i.e.,

$$L_\star^{(k)}(\theta_k,\theta_0) = \rho_k \tag{20}$$

the above two equations are combined to result in an equation which is used to solving μ_k as

$$\mathbf{z}_k^{\mathrm{H}}\mathbf{Q}_k\mathbf{z}_k = 0 \tag{21}$$

where

$$\mathbf{z}_k = [1\ \ \mu_k]^{\mathrm{T}} \tag{22}$$

and $\mathbf{Q}_k$ is a 2×2 Hermitian matrix which can be expressed by (23) at the bottom of the page, where $P_\star^{(k-1)}(\theta_k)$ and $P_\star^{(k-1)}(\theta_0)$ stand for the power response at θ_k and θ_0 of $(k-1)$th step, respectively, as $P_\star^{(k-1)}(\theta_k) = |\mathbf{w}_{k-1}^{\mathrm{H}}\mathbf{a}(\theta_k)|^2$ and $P_\star^{(k-1)}(\theta_0) = |\mathbf{w}_{k-1}^{\mathrm{H}}\mathbf{a}(\theta_0)|^2$. In (23), d_k is a complex-valued number as

$$d_k = \mathbf{w}_{k-1}^{\mathrm{H}}\mathbf{a}(\theta_k)\|\mathbf{a}(\theta_k)\|_2^2 - \rho_k\mathbf{w}_{k-1}^{\mathrm{H}}\mathbf{a}(\theta_0)v(\theta_k,\theta_0) \tag{24}$$

which can be determined by $\mathbf{w}_{k-1}$, $\mathbf{a}(\theta_0)$, $\mathbf{a}(\theta_k)$ and ρ_k.

Obviously, let $\widehat{\mathbf{z}}_k$ be a solution to (21) and assume that $\widehat{\mathbf{z}}_k(1)\neq 0$, it can be readily concluded that

$$\mu_k = \mathbf{z}_k(2) = \widehat{\mathbf{z}}_k(2)/\widehat{\mathbf{z}}_k(1) \tag{25}$$

where $\mathbf{z}_k(i)$ is the ith element of a vector $\mathbf{z}_k$. It is known that if $\mathbf{Q}_k = \mathbf{O}$ then $\widehat{\mathbf{z}}_k$ could be an arbitrary vector. However, in this case, we have $P_\star^{(k-1)}(\theta_k) - \rho_k P_\star^{(k-1)}(\theta_0) = 0$. In other words, we have $L_\star^{(k-1)}(\theta_k,\theta_0) = P_\star^{(k-1)}(\theta_k)/P_\star^{(k-1)}(\theta_0) = L_\star^{(k)}(\theta_k,\theta_0) = \rho_k$. This implies that $\mathbf{w}_{k-1}$ has satisfied the response requirement at θ_k, and hence, $\mu_k = 0$ is taken. Therefore, we only consider the case of $\mathbf{Q}_k \neq \mathbf{O}$, i.e., there must exist at least one non-zero eigenvalue.

The determinant of $\mathbf{Q}_k$ is shown in (26) at the bottom of the page. We show that $\widehat{\mathbf{z}}_k$ and hence μ_k can be determined from the eigenvectors of $\mathbf{Q}_k$. Let the eigenvalue decomposition (EVD) of $\mathbf{Q}_k$ be denoted as

$$\mathbf{Q}_k = \mathbf{U}_k\mathbf{\Lambda}_k\mathbf{U}_k^{\mathrm{H}} \tag{27}$$

where $\mathbf{U}_k$ is an unitary matrix given by $\mathbf{U}_k = \left[\begin{smallmatrix} u_{11} & u_{12} \\ u_{21} & u_{22}\end{smallmatrix}\right]$, and $\mathbf{\Lambda}_k = \mathrm{diag}\,([\lambda_1,\lambda_2])$ with λ_1 and λ_2 being the eigenvalues of $\mathbf{Q}_k$, $\mathrm{diag}\,([\lambda_1,\lambda_2])$ stands for a diagonal matrix with the diagonals given by λ_1 and λ_2. According to (26), we have $\lambda_1\lambda_2 = \det(\mathbf{Q}_k) \le 0$. Substituting (27) into (21), we have

$$\widehat{\mathbf{z}}_k^{\mathrm{H}}\mathbf{U}_k\mathbf{\Lambda}_k\mathbf{U}_k^{\mathrm{H}}\widehat{\mathbf{z}}_k = \mathbf{y}_k^{\mathrm{H}}\mathbf{\Lambda}_k\mathbf{y}_k = \lambda_1|y_1|^2 + \lambda_2|y_2|^2 = 0 \tag{28}$$

where

$$\mathbf{y}_k \triangleq \mathbf{U}_k^{\mathrm{H}}\widehat{\mathbf{z}}_k = [y_1\ \ y_2]^{\mathrm{T}}. \tag{29}$$

Without loss of generality, assume that λ_2 is non-zero, and hence, we have $|y_2/y_1| = \sqrt{-\lambda_1/\lambda_2}$, and $\mathbf{y}_k$ can be further rewritten as

$$\mathbf{y}_k = \kappa\left[1\ \ \sqrt{-\lambda_1/\lambda_2}e^{j\phi}\right]^{\mathrm{T}} \tag{30}$$

where κ is a nonzero complex-valued number and $\phi\in\mathbb{R}$. As a result, the solution to (21) can be expressed as

$$\widehat{\mathbf{z}}_k = \mathbf{U}_k\mathbf{y}_k = \kappa\begin{bmatrix} u_{11}+\sqrt{-\lambda_1/\lambda_2}u_{12}e^{j\phi} \\ u_{21}+\sqrt{-\lambda_1/\lambda_2}u_{22}e^{j\phi}\end{bmatrix} \tag{31}$$

and μ_k has the following form:

$$\mu_k = \frac{\widehat{\mathbf{z}}_k(2)}{\widehat{\mathbf{z}}_k(1)} = \frac{u_{21}+\sqrt{-\lambda_1/\lambda_2}u_{22}e^{j\phi}}{u_{11}+\sqrt{-\lambda_1/\lambda_2}u_{12}e^{j\phi}} \tag{32}$$

provided that $u_{11}+\sqrt{-\lambda_1/\lambda_2}u_{12}e^{j\phi}\neq 0$. Let $\mathbb{F}$ denotes the set of ϕ as

$$\mathbb{F} = \left\{\phi\middle| u_{11}+\sqrt{-\lambda_1/\lambda_2}u_{12}e^{j\phi}\neq 0\right\} \tag{33}$$

then it can be verified that for any $\phi\in\mathbb{F}\subset\mathbb{R}$, $[1\ \ \mu_k]^{\mathrm{T}}$ with μ_k obtained as (32) must be a solution to (21).

Remark 1: As a matter of fact, in general we have $\mathbb{F}=\mathbb{R}$. This can be inferred from (78) in Appendix B, where it is shown that if $\mathbf{Q}_k(2,2)\neq 0$, we have $|u_{11}|^2 \neq -(\lambda_1/\lambda_2)|u_{12}|^2$, then $u_{11}+\sqrt{-\lambda_1/\lambda_2}u_{12}e^{j\phi}\neq 0$ for any $\phi\in\mathbb{R}$. From (23), it can be concluded that if $\|\mathbf{a}(\theta_k)\|_2^4 \neq \rho_k|v(\theta_k,\theta_0)|^2$, then $\mathbb{F}=\mathbb{R}$.

$$\begin{aligned}\mathbf{Q_k} &= \left[\mathbf{w_{k-1}}\quad \mathbf{a}(\theta_k)\right]^{\mathrm{H}}\left(\mathbf{a}(\theta_k)\mathbf{a}^{\mathrm{H}}(\theta_k) - \rho_k\mathbf{a}(\theta_0)\mathbf{a}^{\mathrm{H}}(\theta_0)\right)\left[\mathbf{w_{k-1}}\ \mathbf{a}(\theta_k)\right] \\ &= \begin{bmatrix} P_\star^{(k-1)}(\theta_k) - \rho_k P_\star^{(k-1)}(\theta_0) & d_k \\ d_k^* & \|\mathbf{a}(\theta_k)\|_2^4 - \rho_k|v(\theta_k,\theta_0)|^2\end{bmatrix}\end{aligned} \tag{23}$$

$$\begin{aligned}\det(\mathbf{Q}_k) &= \left(P_\star^{(k-1)}(\theta_k) - \rho_k P_\star^{(k-1)}(\theta_0)\right)\left(\|\mathbf{a}(\theta_k)\|_2^4 - \rho_k|v(\theta_k,\theta_0)|^2\right) - |d_k|^2 \\ &= -\rho_k\left(P_\star^{(k-1)}(\theta_0)\|\mathbf{a}(\theta_k)\|_2^4 + P_\star^{(k-1)}(\theta_k)|v(\theta_k,\theta_0)|^2 - 2\mathrm{Re}\left(\mathbf{w}_{k-1}^{\mathrm{H}}\mathbf{a}(\theta_0)\mathbf{a}^{\mathrm{H}}(\theta_k)\mathbf{w}_{k-1}\|\mathbf{a}(\theta_k)\|_2^2 v(\theta_k,\theta_0)\right)\right) \\ &= -\rho_k|\mathbf{w}_{k-1}^{\mathrm{H}}\mathbf{a}(\theta_0)\|\mathbf{a}(\theta_k)\|_2^2 - \mathbf{w}_{k-1}^{\mathrm{H}}\mathbf{a}(\theta_k)v^*(\theta_k,\theta_0)|^2 \\ &\le 0\end{aligned} \tag{26}$$

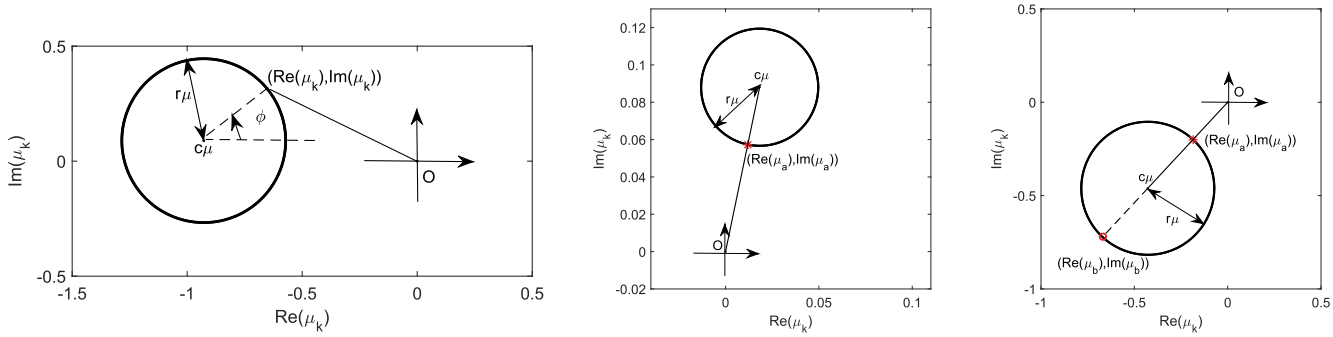

(a) (b) (c)

Fig. 4. Geometric distribution of μ_k. (a) Illustration of μ_k. (b) Distribution of μ_k satisfying $L_\star(20^\circ, 0^\circ) = -30$ dB. (c) Distribution of μ_k satisfying $L_\star(-2^\circ, 0^\circ) = -2$ dB.

In fact, the case $\|\mathbf{a}(\theta_k)\|_2^4 = \rho_k |v(\theta_k, \theta_0)|^2$ is seldom encountered in practical application. This is because $\|\mathbf{a}(\theta_k)\|_2^4 = \rho_k |v(\theta_k, \theta_0)|^2$ yields $\rho_k = \frac{\|\mathbf{a}(\theta_k)\|_2^4}{|v(\theta_k, \theta_0)|^2}$, which is the quiescent normalized response $L_0(\theta_k, \theta_0)$ when taking the weight vector as $\mathbf{a}(\theta_k)$. Note that the response is normalized by the output at θ_0 but its beam center points to θ_k, so we have $\rho_k > 1$ in this case. We say that this situation barely happens, because that if θ_0 denotes the beam center, we hardly adjust the level at θ_k, where $\theta_k \neq \theta_0$, to be higher than the output at θ_0.

C. Weight Vector Determination via Geometrical Approach

From (32), we know that there exists infinitely many μ_k that make (20) hold, the determination of μ_k can be accomplished by the aid of EVD. To further simplify the procedure of solving μ_k, and more importantly, to have a geometrical insight into the distribution of μ_k, another elegant approach is introduced. To begin with, the following proposition is needed.

Proposition 1: For any $a_1, a_2, b_1, b_2 \in \mathbb{C}$, a complex number c satisfies

$$c = \frac{a_1 + a_2 e^{j\phi}}{b_1 + b_2 e^{j\phi}} \tag{34}$$

where ϕ can be altered in the set $\mathbb{D} = \{\phi | b_1 + b_2 e^{j\phi} \neq 0\}$. Then $\mathbb{G}$, which denotes the trajectory set of $[\mathrm{Re}(c) \;\; \mathrm{Im}(c)]^{\mathrm{T}}$, is the set or subset of circle $\mathbb{C}_0$, the center point of $\mathbb{C}_0$ is

$$\mathbf{c}_0 = \frac{1}{h_b} \mathbf{B} \mathbf{a}_\star \tag{35}$$

and the radius r_c of the circle satisfies

$$r_c^2 = \frac{1}{h_b^2} \mathbf{a}_\star^{\mathrm{T}} \mathbf{B}^{\mathrm{T}} \mathbf{B} \mathbf{a}_\star - \frac{h_a}{h_b} \tag{36}$$

where $\mathbf{a}_\star = \begin{bmatrix} \mathbf{a}_1^{\mathrm{T}} & -\mathbf{a}_2^{\mathrm{T}} \end{bmatrix}^{\mathrm{T}}$, $\mathbf{a}_l = \begin{bmatrix} \mathrm{Re}(a_l) & \mathrm{Im}(a_l) \end{bmatrix}^{\mathrm{T}}$, $\mathbf{B} = \begin{bmatrix} \mathbf{b_1} & \mathbf{P}\mathbf{b}_1 & \mathbf{b}_2 & \mathbf{P}\mathbf{b}_2 \end{bmatrix}$, $\mathbf{b}_l = \begin{bmatrix} \mathrm{Re(b_l)} & -\mathrm{Im}(b_l) \end{bmatrix}^{\mathrm{T}} (l = 1, 2)$, $\mathbf{P} = \begin{bmatrix} 0 & -1 \\ 1 & 0 \end{bmatrix}$, $h_a = \mathbf{a}_1^{\mathrm{T}} \mathbf{a}_1 - \mathbf{a}_2^{\mathrm{T}} \mathbf{a}_2$, $h_b = \mathbf{b}_1^{\mathrm{T}} \mathbf{b}_1 - \mathbf{b}_2^{\mathrm{T}} \mathbf{b}_2$. If $\mathbb{D} = \mathbb{R}$, then $\mathbb{G} = \mathbb{C}_0$, otherwise, $\mathbb{G} \subseteq \mathbb{C}_0$.

Proof: See Appendix A. ■

Applying Proposition 1 to (32), we can obtain the following proposition, which is crucial and enables us to find out all the solutions to μ_k that meet the requirement (20) in a more simple and intuitive manner.

Proposition 2: Assuming that ϕ in (32) altering in the set $\mathbb{F}$, then the trajectory set of $\begin{bmatrix} \mathrm{Re}(\mu_k) & \mathrm{Im}(\mu_k) \end{bmatrix}^{\mathrm{T}}$ is a circle $\mathbb{C}_\mu$ or subset of $\mathbb{C}_\mu$, with center point

$$\mathbf{c}_\mu = \frac{1}{\mathbf{Q}_k(2,2)} \begin{bmatrix} -\mathrm{Re}(\mathbf{Q}_k(1,2)) \\ \mathrm{Im}(\mathbf{Q}_k(1,2)) \end{bmatrix} \tag{37}$$

and a radius of

$$r_\mu = \frac{\sqrt{-\det(\mathbf{Q}_k)}}{|\mathbf{Q}_k(2,2)|} \tag{38}$$

Proof: Proposition 2 is a consequence of Proposition 1 with $a_1 = u_{21}$, $a_2 = \sqrt{-\lambda_1/\lambda_2} u_{22}$, and $b_1 = u_{11}$, $b_2 = \sqrt{-\lambda_1/\lambda_2} u_{12}$. The detailed proof is given in Appendix B. ■

As expected, Proposition 2 describes the trajectory of μ_k. Let us define a function g as

$$g(\mathbf{v}) = \mathbf{v}(1) + j\mathbf{v}(2) \tag{39}$$

where $\mathbf{v}$ is a 2×1 vector. Thus, for any $\phi \in \mathbb{F}$, we have

$$\begin{aligned} \mu_k &= g\left(\begin{bmatrix} \mathbf{c}_\mu(\mathbf{1}) + \mathbf{r}_\mu \cos\phi \;\; \mathbf{c}_\mu(2) + r_\mu \sin\phi \end{bmatrix}^{\mathrm{T}} \right) \\ &= -\frac{\mathbf{Q}_k^*(1,2)}{\mathbf{Q}_k(2,2)} + \frac{\sqrt{-\det(\mathbf{Q}_k)}}{|\mathbf{Q}_k(2,2)|} e^{j\phi} \end{aligned} \tag{40}$$

which satisfies the specific condition (20). Note that (40) is equivalent to (32), but it can obtain μ_k in a simpler way without EVD. In addition, it illustrates μ_k geometrically as in Fig. 4(a). This helps us to find some latent characteristics more clearly as shown below.

D. Selection of μ_k

It has been shown that we have infinitely many solutions of μ_k to fulfill the specific requirement (20). A natural question is that will all solutions result in the same performance? If not, with which criterion the solution should be selected to achieve the desired array response? In fact, in the above analysis, we have not taken into account the possible change of the response

at θ_{k-1} if we modify the weight vector $\mathbf{w}_{k-1}$ to $\mathbf{w}_k$ to satisfy the desired response at θ_k. Therefore, an ideal criterion is that designing $\mathbf{w}_k$ (or equivalently selecting μ_k) to achieve the desired response at θ_k while the responses at any other directions remain unchanged. Mathematically, this can be described as

$$\begin{cases} L_\star^{(k)}(\theta,\theta_0) = \rho_k, & \text{for } \theta = \theta_k \\ L_\star^{(k)}(\theta,\theta_0) = L_\star^{(k-1)}(\theta,\theta_0), & \text{for } \theta \neq \theta_k. \end{cases} \tag{41}$$

Undoubtedly, such an criterion cannot be achieved, since the array response is a continuous function. Nevertheless, (41) provides a useful guideline to design a pattern with practically satisfactory performance. Thus, we formulate the problem of response control as follows

$$\begin{aligned} \min_{\mu_k} \quad & \int_{\theta\neq\theta_k} \left| L_\star^{(k)}(\theta,\theta_0) - L_\star^{(k-1)}(\theta,\theta_0) \right| d\theta \\ \text{s.t.} \quad & L_\star^{(k)}(\theta_k,\theta_0) = \rho_k. \end{aligned} \tag{42}$$

In fact, (42) can be equivalently expressed as

$$\begin{aligned} \min_{\mu_k} \quad & \int_{\theta\in\Omega} \left| L_\star^{(k)}(\theta,\theta_0) - L_\star^{(k-1)}(\theta,\theta_0) \right| d\theta \\ \text{s.t.} \quad & L_\star^{(k)}(\theta_k,\theta_0) = \rho_k \end{aligned} \tag{43}$$

where Ω denotes the whole angle sector. A common approach to tackling the integration is using discretization. The discrete form of (42) is given by

$$\begin{aligned} \min_{\mu_k} \quad & \sum_{\theta\neq\theta_k} \left| L_\star^{(k)}(\theta,\theta_0) - L_\star^{(k-1)}(\theta,\theta_0) \right| \\ \text{s.t.} \quad & L_\star^{(k)}(\theta_k,\theta_0) = \rho_k. \end{aligned} \tag{44}$$

The above optimization problem can be optimally solved by global search, i.e., by tuning ϕ from 0 to 2π. Of course, this approach has the known drawback of high computational complexity. Nevertheless, the result of global search is helpful to demonstrate some implicit characteristics about the best μ_k, and further gives us enlightenment to design the optimal solution in a simple way. Therefore, we carry out an example to examine the performance change when altering μ_k on $\mathbb{C}_\mu$ or equivalently sliding ϕ on $[0, 2\pi]$.

Here, a ULA of 16 isotropic elements is used, the angle sector is $\Omega = [-90°, 90°]$, the initial weight vector is $\mathbf{w}_0 = \mathbf{a}(\theta_0)$, where θ_0 is fixed at $0°$. We set $k = 1$ and $\theta_k = 20°$, and aim to synthesize a pattern with $L_\star(20°, 0°) = -30$ dB. The distribution of μ_k can be found in Fig. 4(b). In this case, we can figure out $\mathbf{c}_\mu = \begin{bmatrix} 0.0183 & 0.0881 \end{bmatrix}^{\mathrm{T}}$ and $r_\mu = 0.0314$.

To measure the performance of different μ_k on $\mathbb{C}_\mu$, we uniformly discretize the corresponding pattern of each μ_k into I points and define the cost function at the kth step as

$$J \triangleq \frac{1}{I}\sum_{i=1}^{I} \left| L_\star^{(k)}(\theta_i,\theta_0) - L_\star^{(k-1)}(\theta_i,\theta_0) \right|. \tag{45}$$

Obviously, it is seen that J measures the average deviation between $L_\star^{(k)}(\theta,\theta_0)$ and $L_\star^{(k-1)}(\theta,\theta_0)$. In this example, we uniformly sample Ω every $0.02°$ and hence obtain 9001 discrete points, i.e., $I = 9001$. Fig. 5 shows the curves of J versus ϕ.

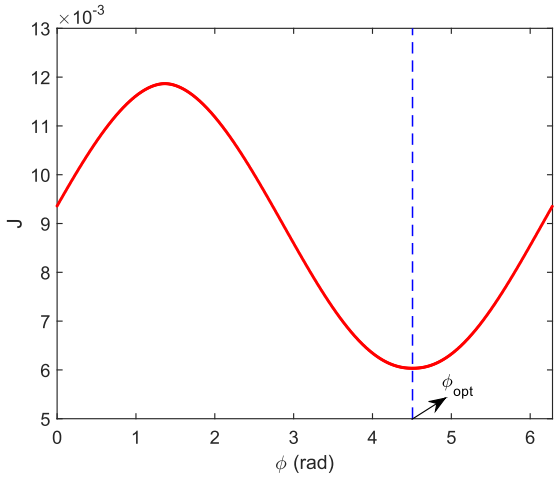

Fig. 5. J versus ϕ ($L_\star(20°, 0°) = -30$ dB).

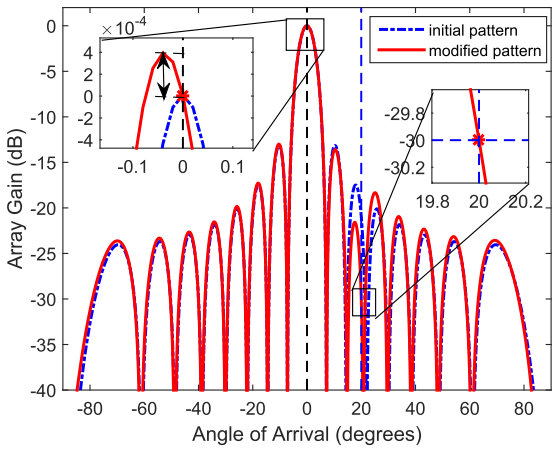

Fig. 6. Response pattern when taking $\mu_k = 0.0119 + j0.0573$.

Here, ϕ is the argument relative to $(\mathrm{Re}(\mathbf{c}_\mu) \;\; \mathrm{Im}(\mathbf{c}_\mu))$ and its geometric meaning has been shown in Fig. 4(a).

From Fig. 5, we notice that J achieves the minimum value at $\phi_{opt} = 4.5077$ rad. A brief anlysis gives that $\pi < \phi_{opt} < 1.5\pi$ in this case. Combining Fig. 4(b), we find that the optimal μ_{opt} is located relatively near to original point, where

$$\mu_{opt} \triangleq \mu_k|_{\phi=\phi_{opt}}. \tag{46}$$

This observation implies that a μ_k with relatively less module value may lead to a relatively lower cost function, and finally generate a pattern with better performance.

To illustrate the rationality of above inference, we compare the performance when μ_k is set to be with different module. To be specific, the first approach takes μ_k as $0.0119 + j0.0573$ and the second approach chooses $\mu_k = 0.0247 + j0.1188$, their module value are 0.0586 and 0.1213, respectively. We can test that in both cases, μ_k locates on the circle plotted in Fig. 4(b). The corresponding patterns have been normalized by the power output at θ_0, and are shown in Figs. 6 and 7, respectively. From Figs. 6 and 7, it is observed that in both cases $L_\star(20°, 0°)$ get their desired values. However, the locations of the maximum values have been shifted slightly in both

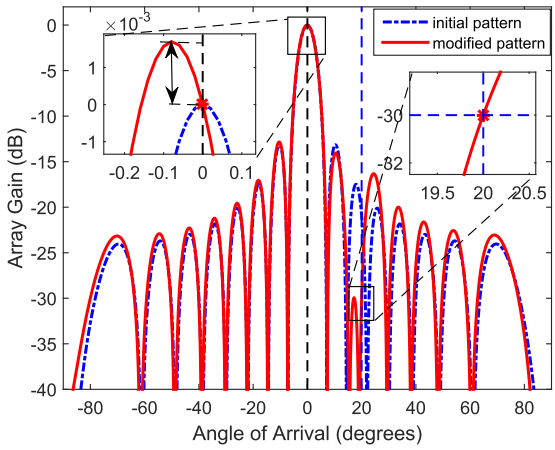

Fig. 7. Response pattern when taking $\mu_k = 0.0247 + j0.1188$.

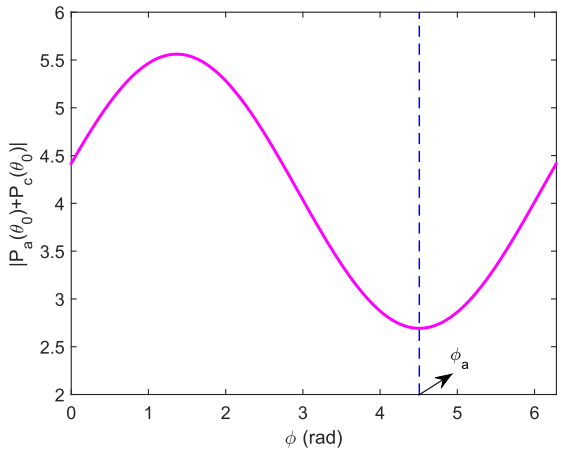

Fig. 8. $|P_a(\theta_0) + P_c(\theta_0)|$ versus ϕ ($L_\star(20°, 0°) = -30$ dB).

cases. More precisely, in the first case, it is seen that the peak value is about $L_\star(-0.04°, 0°) = 4 \times 10^{-4}$ dB. While in the seconde case, the maximum value of the pattern is about $L_\star(-0.07°, 0°) = 1.9 \times 10^{-3}$ dB.

In summary, we deduce that the μ_k with a smaller module value may lead to less pattern distortion. As a consequence, by setting μ with the smallest module value, the corresponding pattern may perform best. In the sequel, we will give a more theoretical explanation and further propose a tip that is both simple and effective to select an appropriate μ_k.

Recalling the $\mathbf{w}_k$ and $\mathbf{w}_{k-1}$, we have

$$L_\star^{(k-1)}(\theta, \theta_0) = \frac{P_\star^{(k-1)}(\theta)}{P_\star^{(k-1)}(\theta_0)} = \frac{|\mathbf{w}_{k-1}^{\mathrm{H}}\mathbf{a}(\theta)|^2}{|\mathbf{w}_{k-1}^{\mathrm{H}}\mathbf{a}(\theta_0)|^2} \tag{47}$$

$$\begin{aligned} L_\star^{(k)}(\theta, \theta_0) &= \frac{P_\star^{(k)}(\theta)}{P_\star^{(k)}(\theta_0)} = \frac{|\mathbf{w}_k^{\mathrm{H}}\mathbf{a}(\theta)|^2}{|\mathbf{w}_k^{\mathrm{H}}\mathbf{a}(\theta_0)|^2} \\ &= \frac{P_i^{(k)}(\theta) + P_a^{(k)}(\theta) + P_c^{(k)}(\theta)}{P_i^{(k)}(\theta_0) + P_a^{(k)}(\theta_0) + P_c^{(k)}(\theta_0)} \end{aligned} \tag{48}$$

where $P_\star^{(k)}(\theta)$ denotes the power response at θ in the kth step. In (48), $P_i^{(k)}(\theta) \triangleq |\mathbf{w}_{k-1}^{\mathrm{H}}\mathbf{a}(\theta)|^2$, $P_a^{(k)}(\theta) \triangleq |\mu_k^* v(\theta, \theta_k)|^2$, $P_c^{(k)}(\theta) \triangleq 2\mathrm{Re}(\mu_k \mathbf{w}_{k-1}^{\mathrm{H}}\mathbf{a}(\theta)v(\theta_k, \theta))$. From (47), we can rewrite $L_\star^{(k-1)}(\theta, \theta_0)$ as

$$L_\star^{(k-1)}(\theta, \theta_0) = \frac{P_i^{(k)}(\theta)}{P_i^{(k)}(\theta_0)}. \tag{49}$$

Therefore, in order to make the pattern distortion $|L_\star^{(k)}(\theta, \theta_0) - L_\star^{(k-1)}(\theta, \theta_0)|$ sufficiently small, we should select a μ_k such that $\frac{P_i^{(k)}(\theta)+P_a^{(k)}(\theta)+P_c^{(k)}(\theta)}{P_i^{(k)}(\theta_0)+P_a^{(k)}(\theta_0)+P_c^{(k)}(\theta_0)}$ approximates to $\frac{P_i^{(k)}(\theta)}{P_i^{(k)}(\theta_0)}$. Naturally, this can be achieved by enforcing both $|P_a^{(k)}(\theta) + P_c^{(k)}(\theta)|$ and $|P_a^{(k)}(\theta_0) + P_c^{(k)}(\theta_0)|$ as small as possible. According to the definition of $P_a^{(k)}(\theta)$ and $P_c^{(k)}(\theta)$ given above, they can be rewritten as $P_a^{(k)}(\theta) = |\mu_k|^2|v(\theta_k, \theta)|^2$ and $P_c^{(k)}(\theta) = 2|\mu_k||v(\theta_k, \theta)|\gamma_k$, respectively, where $\gamma_k = |\mathbf{w}_{k-1}^{\mathrm{H}}\mathbf{a}(\theta)|\cos(\varphi_k)$ with $\varphi_k = \angle(\mu_k \mathbf{w}_{k-1}^{\mathrm{H}}\mathbf{a}(\theta)v(\theta_k, \theta))$, here $\angle(\cdot)$ returns the argument of a complex number, the scope of argument is $[0, 2\pi)$. Therefore, $|P_a^{(k)}(\theta) + P_c^{(k)}(\theta)|$ can be re-expressed as

$$|P_a^{(k)}(\theta) + P_c^{(k)}(\theta)| = |v(\theta_k, \theta)|^2 \left| |\mu_k|^2 + \frac{2\gamma_k|\mu_k|}{|v(\theta_k, \theta)|} \right|. \tag{50}$$

Obviously, it is seen that, in order to obtain relatively smaller values of both $|P_a^{(k)}(\theta) + P_c^{(k)}(\theta)|$ and $|P_a^{(k)}(\theta_0) + P_c^{(k)}(\theta_0)|$, we should select a μ_k with smallest modulus among $\mathbb{C}_\mu$.

From Fig. 4(a), we know the nearest point to origin point among all points on the circle $\mathbb{C}_\mu$, is the intersection of circle $\mathbb{C}_\mu$ and the line which passes the origin and center $\mathbf{c}_\mu$. Defining

$$\phi_a \triangleq \mathrm{mod}(\angle g(\mathbf{c}_\mu) + \pi, 2\pi), \quad \mu_a \triangleq \mu_k|_{\phi=\phi_a} \tag{51}$$

where $\mathrm{mod}(a, b)$ denotes the modulo operator on a by b. Then a short analysis gives that

$$\mu_a = \arg \min_{\mu_k \in \mathbb{C}_\mu} |\mu_k| = g\left(\frac{|\mathbf{c}_\mu| - r_\mu}{|\mathbf{c}_\mu|}\mathbf{c}_\mu\right). \tag{52}$$

The coordinates of μ_a can be found in Fig. 4(b).

To further illustrate its rationality, the curve of $|P_a^{(k)}(\theta_0) + P_c^{(k)}(\theta_0)|$ versus ϕ is depicted in Fig. 8 given the same settings of the previous example. It is seen that $|P_a^{(k)}(\theta_0) + P_c^{(k)}(\theta_0)|$ achieves the minimum at $\phi = \phi_a$. Furthermore, from (51) we can figure out $\phi_a = 4.5077$ rad. In fact, this is also the optimal value we have obtained by global search in the above test example. Therefore, $\mu_a = \mu_{opt}$ in this case. This agrees with the theoretical analysis above, meanwhile, it gives the rational explanation of setting μ as μ_a to obtain a pattern with well performance. Additionally, it is interesting to note that in this scenario we can further figure out $\mu_a = 0.0119 + j0.0573$, which coincides with the results shown in Fig. 2.

From the above test and analysis, it is found that a satisfactory pattern can be obtained by setting μ as μ_a. Note that although μ_a in (52) may not be the optimal solution to the original optimization problem (43) or (44), it can result in a sufficiently small cost value in (43) or (44). Thus, the choice of μ_a as (52) is still meaningful and can offer satisfactory performance as shown in our simulations.

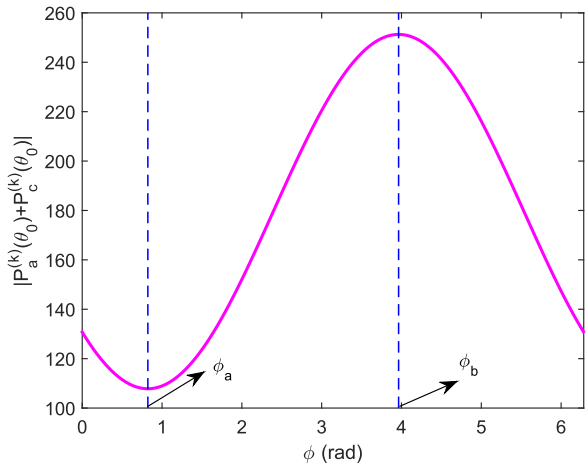

Fig. 9. $|P_a^{(k)}(\theta_0) + P_c^{(k)}(\theta_0)|$ versus ϕ ($L_\star(-2°, 0°) = -2$ dB).

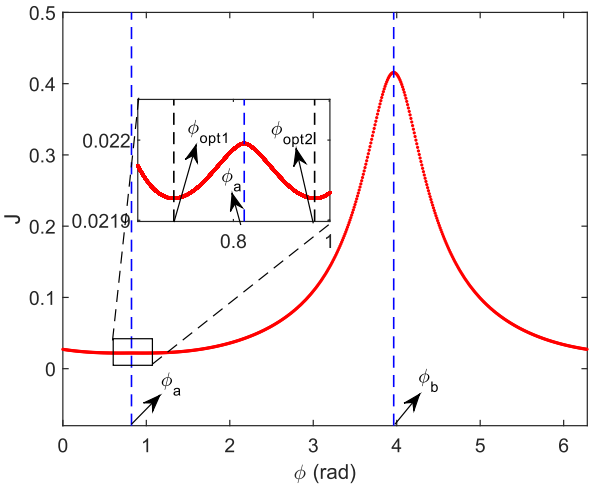

Fig. 10. J versus ϕ ($L_\star(-2°, 0°) = -2$ dB).

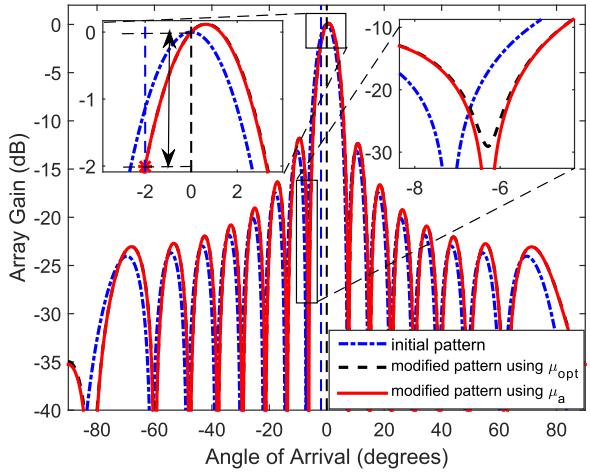

Fig. 11. Response patterns comparison.

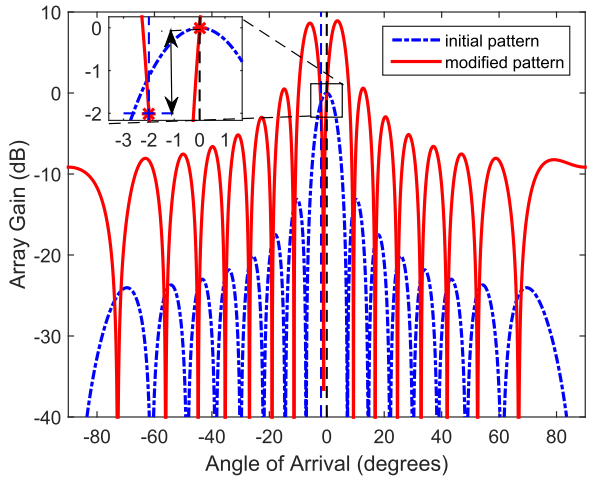

Fig. 12. Response pattern when taking μ_k as μ_b in Fig. 4(c).

In the above example, the effectiveness of the proposed method is shown by sidelobe response control. To further demonstrate the performance, an additional example is carried out to control response in mainlobe region. Here, $\theta_k = -2°$, it is required to adjust its normalized response to -2 dB, other parameters are same as the previous example. It can be calculated that $\mathbf{c}_\mu = \begin{bmatrix} -0.4280 & -0.4608 \end{bmatrix}^{\mathrm{T}}$, $r_\mu = 0.3562$, $\phi_a = 0.8223$ rad. For the purpose of simulation comparison, we test the performance of another choice of ϕ, that is ϕ_b, which satisfies

$$\phi_b \triangleq \angle g(\mathbf{c}_\mu). \tag{53}$$

It can be found that μ_k obtains its maximum module value by setting μ_k as $\mu_b \triangleq \mu_k|_{\phi=\phi_b}$. We can calculate that $\phi_b = 3.9639$ rad in this example.

Fig. 4(c) displays the distribution of μ_k, the locations of μ_a and μ_b are also shown there. Figs. 9 and 10 display $|P_a^{(k)}(\theta_0) + P_c^{(k)}(\theta_0)|$ and J versus ϕ, respectively. It is seen that both $|P_a^{(k)}(\theta_0) + P_c^{(k)}(\theta_0)|$ and J obtain their maximum values as $\phi = \phi_b$. In addition, when $\phi = \phi_a$, $|P_a^{(k)}(\theta_0) + P_c^{(k)}(\theta_0)|$ reaches its minimum while J does not. In other words, μ_a is not the optimal solution to (43) or (44) in this scenario. Nevertheless, it is seen from Fig. 10 that the value of cost function at ϕ_a is actually sufficiently small. Moreover, from Fig. 10 we find that there exists two optimal solutions to minimize J, the corresponding optimal ϕ equals to $\phi_{opt1} = 0.6754$ rad and $\phi_{opt2} = 0.9692$ rad. Then the optimal pattern can be obtained by setting $\phi = \phi_{opt1}$ or $\phi = \phi_{opt2}$.

The synthesized patterns when setting μ_k as μ_a and μ_b are shown in Figs. 11 and 12, respectively. Obviously, in both cases, we have $L_\star(-2°, 0°) = -2$ dB. However, the corresponding pattern in Fig. 12 has been distorted seriously, it forms a notch near θ_0. In order to examine the difference between the patterns when taking $\mu_k = \mu_a$ and $\mu_k = \mu_{opt}$. Fig. 11 also displays the optimal array response by setting $\mu_k = \mu_{opt}$. It is interesting to note that the two optimal solutions obtain a same beam pattern, so here the only one optimal pattern is demonstrated. It can be seen that the synthesized pattern when setting $\mu_k = \mu_a$ is almost the same as the optimal pattern. The second example also validates the effectiveness of choosing μ_k by (52).

TABLE I
SUMMARY OF A^{2}RC BASED PATTERN SYNTHESIS

Input	$k=0$, θ_0, $\mathbf{w}_0$, Ω_m, Ω_s, $L_d(\theta)$, $L_\star^{(0)}(\theta)=\frac{\lvert\mathbf{w}_0^{\mathrm{H}}\mathbf{a}(\theta)\rvert^2}{\lvert\mathbf{w}_0^{\mathrm{H}}\mathbf{a}(\theta_0)\rvert^2}$
Step 1.	Set $k=k+1$, find the reference angle $\theta_0^{(k-1)}$ that has maximum value of $L_\star^{(k-1)}(\theta)$ using (54).
Step 2.	**Mainlobe control**: Find the angle θ_k at which $L_\star^{(k-1)}(\theta)$ deviates most from $L_d(\theta)$ in mainlobe region using (55). **Sidelobe control**: Determine the $\tilde{\Omega}_s^{(k)}$ as (56) and find out θ_k as (57).
Step 3.	Compute $\mathbf{Q}_k$ with $\theta_0^{(k)}$, θ_k, $L_d(\theta_k)$ and $\mathbf{w}_{k-1}$, and then calculate μ_a using (52).
Step 4.	Update $\mathbf{w}_k=\mathbf{w}_{k-1}+\mu_a\mathbf{a}(\theta_k)$ and $L_\star^{(k)}(\theta)=\frac{\lvert\mathbf{w}_k^{\mathrm{H}}\mathbf{a}(\theta)\rvert^2}{\max\{\lvert\mathbf{w}_k^{\mathrm{H}}\mathbf{a}(\theta)\rvert^2\}}$
Step 5.	Go to **Step 1** unless the pattern is satisfactorily synthesized.
Output	$\mathbf{w}_k$ and $L_\star^{(k)}(\theta)$.

Now we can select a relative suitable μ_a with low complexity. Despite it may not be the optimal solution to (43) or (44), simulation results indicate that the choice of μ_a as in (52) gets an obvious performance improvement in vast majority cases.

IV. APPLICATION OF A^{2}RC TO PATTERN SYNTHESIS

In the above section, we have devised the A^{2}RC algorithm, which enables us to accurately control the normalized response at a given direction. In what follows, its application to pattern synthesis is discussed. In brief, assuming that the desired pattern is $L_d(\theta)$, it can be synthesized by successively adjusting the normalized response at each angle θ_k to $L_d(\theta_k)$.

A. Considerations for the Application

Prior to the detailed discussion of the application, we have to consider the problem of how to choose the normalized factor and whether it will change along with the step. To this end, we denote by $L_\star^{(k)}(\theta)$ the normalized response after the kth step. It is known that the ideal normalized factor in the kth step should be the maximum response after this step to achieve the accurate response control. Obviously, such a normalized factor is unavailable unless the kth step is completed. Fortunately, as discussed earlier in the A^{2}RC algorithm, the response difference between two consecutive steps is minimized. This implies that the response in the sector excluded the angle being controlled (especially those far away from this angle) would not have significant change. Therefore, in the kth step, the normalized factor can be chosen as $L_\star^{(k)}(\theta_0^{(k-1)})$, where $\theta_0^{(k-1)}$ is the reference angle associated with the maximum normalized response after the $(k-1)$th step. This conclusion can be verified by the results shown in Figs. 6 and 11, in which it is clearly observed that the maximum normalized response are nearly unchanged along with the step.

Remark 2: In fact, the normalized factor can be chosen as $L_\star^{(k)}(\theta_0)$ for a fixed angle θ_0 especially when there are no specific requirements for the mainlobe.

B. Pattern Synthesis Using A^{2}RC

It is seen that in the A^{2}RC algorithm, the weight vector can be analytically obtained in each step, and the sidelobe and mainlobe can be controlled in a very similar manner. More specifically, for the mainlobe control, in the kth step we first determine the angle at which the response is maximum, i.e.,

$$\theta_0^{(k)}=\arg\max_{\theta\in\Omega_m} L_\star^{(k-1)}(\theta) \tag{54}$$

where Ω_m denotes the mainlobe angle sector of the desired pattern. Then, we detect the angle where the response deviates most from the desired one, i.e.,

$$\theta_k=\arg\max_{\theta\in\Omega_m} |L_\star^{(k-1)}(\theta)-L_d(\theta)|. \tag{55}$$

At last, the response at this angle is adjusted using the A^{2}RC algorithm. Such a procedure is terminated until the mainloble response is satisfactorily achieved as desired.

For sidelobe synthesis, in the kth step, we first determine the angle sector at which the response is higher than the desired level as

$$\tilde{\Omega}_s^{(k)}=\{\theta|L_\star^{(k-1)}(\theta)-L_d(\theta)>0,\theta\in\Omega_s\} \tag{56}$$

where Ω_s denotes the whole sidelobe angle sector of the desired pattern. Next, we find out the angle at which the response deviates most from the desired pattern, i.e.,

$$\theta_k=\arg\max_{\theta\in\tilde{\Omega}_s^{(k)}}\left(L_\star^{(k-1)}(\theta)-L_d(\theta)\right). \tag{57}$$

Then, the A^{2}RC algorithm is applied to adjust the response at θ_k to the desired value. The above steps are repeated until the response is satisfactorily synthesized. The A^{2}RC based pattern synthesis approach is summarized in Table I.

Remark 3: In the Step 2 of Table I, we find the angle θ_k by two different ways, according to which region (mainlobe or sidelobe) required to be controlled. When both mainlobe region and sidelobe region are needed to be adjusted, the A^{2}RC algorithm is first applied to synthesize the mainlobe region to the desired pattern, and then to synthesize the sidelobe region. In case that the synthesized mainlobe (sidelobe) pattern is distorted after the sidelobe (mainlobe) synthesis, the A^{2}RC algorithm should be further applied.

C. Comparison With Philip's Method [14]

As discussed above, the proposed A^{2}RC based pattern synthesis approach adjusts the response at each angle successively to the desired value. The proposed method is devised based on the adaptive array theory. In fact, Philip *et al.* also adopted this theory for pattern synthesis in [14]. Philip proposed to assign multiple artificial interferences on peak sidelobe locations. The optimal weight vector is obtained by minimizing the sum of weighted squared errors between synthesized and desired patterns. Iterations on the weighting function in both mainlobe and sidelobe regions insure a desired mainlobe shape as well as desired levels. However, the parameters in Philip's method are selected in an *ad hoc* way. In our proposed method, the parameter of weight vector can be obtained analytically. In brief,

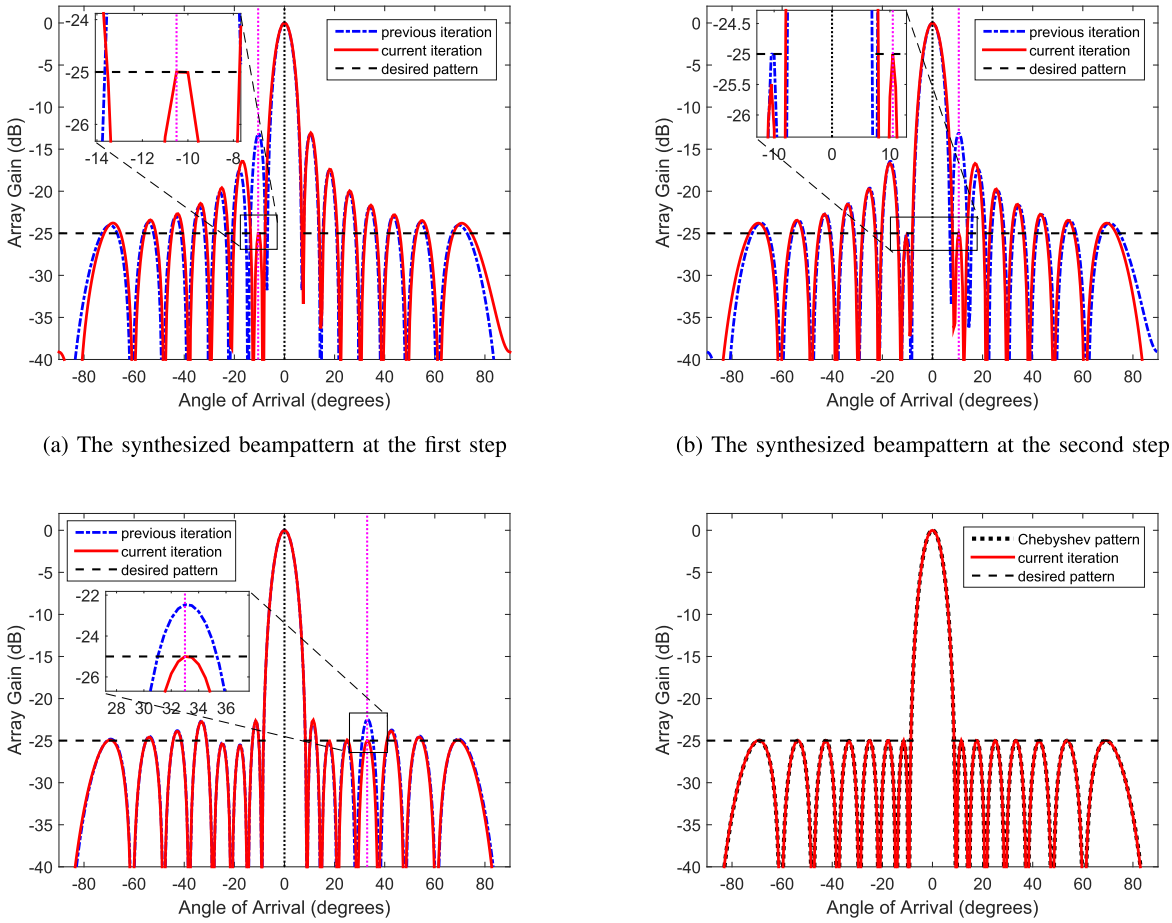

(a) The synthesized beampattern at the first step

(b) The synthesized beampattern at the second step

(c) The synthesized beampattern at the 7-th step

(d) The synthesized beampattern at the 25-th step

Fig. 13. Simulation results for pattern synthesis of uniform sidelobe.

the main difference between the proposed A^{2}RC based pattern synthesis and Philip's method [14] includes:

- In each step, the response at a specific angle can be controlled accurately, while Philip's method does not.
- The proposed method controls pattern successively.
- The INR is altered as an variable that can be either positive or negative, whereas it is required to be nonnegative in Philip's method.
- The proposed method modifies the weight vector successively without matrix inversion, and hence it is computationally attractive.

V. Numerical Results

In this Section, various simulation results are provided to demonstrate the effectiveness of the proposed approach. First, a linear array with isotropic elements is considered. Several examples with different desired patterns are carried out. Next, we consider examples of nonisotropic elements and nonuniform random linear array. Finally, an example to synthesize two-dimensional patterns is given to show the generality of the proposed method.

A. Linear Array With Isotropic Elements

In this subsection, all simulations are carried out by assuming a linear array with isotropic elements. The main beams are steered to $\theta_0 = 0^\circ$ unless otherwise specified.

1) Pattern Synthesis of Uniform Sidelobe: In the first example, a ULA with 16-elements is considered and the desired pattern has uniform sidelobe. The response of the sidelobe is required to be no larger than -25 dB. The synthesis process starts with the initial weight vector $\mathbf{a}(\theta_0)$. Fig. 13 shows the synthesized patterns at different steps.

At the first step, from the initial pattern we find out the location of sidelobe peak whose response deviates most from desired pattern. Let the location be θ_1 and in this example, we have $\theta_1 \approx -10^\circ$ and the response at this direction is controlled by the proposed method. Fig. 13(a) shows the resultant pattern. It is seen that the response at θ_1 is exactly equal to -25 dB.

At the second step, the location of the sidelobe peak (of the resultant pattern after the first step) whose response deviates most from the desired pattern is determined. The angle is $\theta_2 \approx 10^\circ$. By applying the proposed method, the response at θ_2 has been accurately controlled to -25 dB, whereas the response at θ_1 is

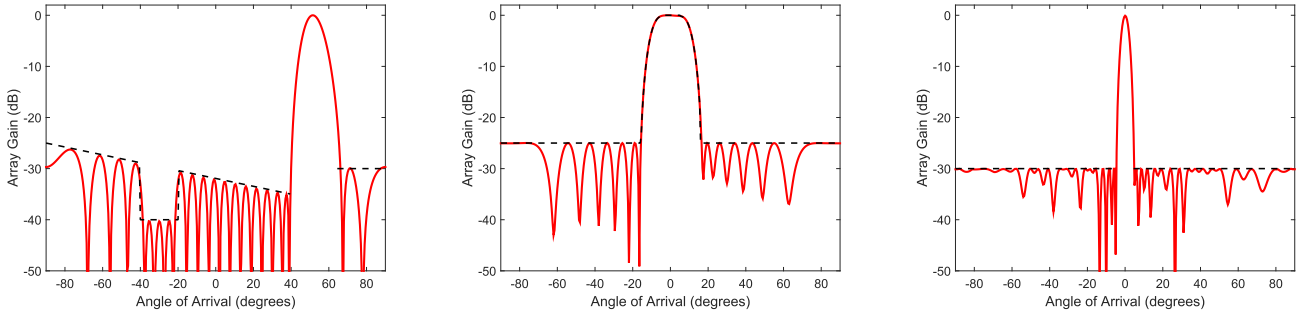

(a) Synthesized pattern with nonuniform sidelobe.

(b) Flat-top pattern.

(c) Low sidelobe pattern using a nonisotropic linear random array.

Fig. 14. Various of patterns synthesized by the proposed method.

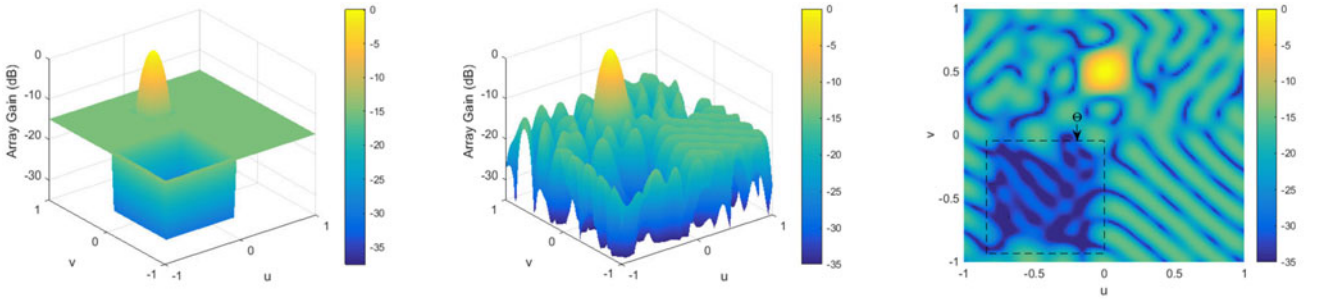

(a) The desired 2-D shape

(b) The 2-D synthesized pattern

(c) Top viem of the 2-D synthesized pattern

Fig. 15. 2-D pattern synthesis with a 10×10 isotropic elements planar array.

almost unchanged as shown in Fig. 13(b). In fact, the response at θ_1 is insignificantly reduced from -25 dB to -25.5 dB. Anyway, the response at this direction meets the requirement of the desired pattern.

According to the proposed method, the above process is repeatedly until the pattern is close enough to the desired pattern. It can be noticed from Fig. 13(c) that after 7 steps all sidelobe levels are very close to the desired level. As shown in Fig. 13(d), after 25 steps, the synthesized beampattern meets the design requirement and is almost same as Chebyshev pattern.

2) Nonuniform Sidelobe Control: Following the example and simulation settings in [12], the desired sidelobe level is assumed to be nonuniform, i.e., it varies with the direction θ. The synthesized pattern is shown in Fig. 14(a), where the desired patterns are shown by dashed lines. Again, it is found that the proposed A^{2}RC based approach performs well.

3) Pattern Synthesis With Constraint in Mainlobe: The third example considers the case where the desired pattern has a flat top in the mainlobe region, which was studied in [14]. Being the same as the first example, a ULA of 16 elements is considered. The mainlobe region of the desired pattern is $[-8^\circ, 8^\circ]$. The sidelobe level is required to be lower than -25 dB. In this case, we first control the mainlobe response to achieve the desired mainlobe pattern and then turn to adjust the sidelobe responses. The resulting pattern is depicted in Fig. 14(b). It is seen that both the mainlobe and side sidelobe can be properly synthesized by the proposed method.

B. Nonisotropic Linear Random Array

In this subsection, we consider a 33-element nonisotropic linear random array, which was described in [4], [12], [13]. The individual pattern for the nth element is given by

$$g_n(\theta) = \frac{\cos\left[\pi l_n \sin(\theta + \tau_n)\right] - \cos(\pi l_n)}{\cos(\theta + \tau_n)} \tag{58}$$

where τ_n and l_n represent the orientation and length of the element. More description of the array can be found in [13]. Fig. 14(c) shows the synthesized pattern in this case and also validates the effectiveness of the A^{2}RC based pattern synthesis method for nonisotropic linear random arrays.

C. Pattern Synthesis for Two-Dimensional Array

In order to demonstrate the generality of the proposed approach, an example of pattern synthesis for two-dimensional array is presented. Without loss of generality, we consider a planar array composed of 10×10 isotropic elements which are spaced by half a wavelength. Fig. 15(a) shows the desired pattern $L_d(u, v)$, where $u = \sin(\theta_e)\cos(\theta_a)$, $v = \sin(\theta_e)\sin(\theta_a)$, and θ_e and θ_a denote elevation and azimuth angles, respectively. The beam steers to $(u_0, v_0) = (0, 0.5)$. The desired sidelobe level inside the set $\Theta = \{(u, v) | -0.8 \le u \le 0, -0.9 \le v \le -0.1\}$ is set to be lower than -30 dB, otherwise it is required to achieve a sidelobe level below -15 dB.

Fig. 15(b) displays the resulting synthesized pattern and Fig. 15(c) plots its top view. It can be seen that the side-

lobe responses both in and outside the region Θ can be correctly controlled. The extensions of the A^{2}RC based pattern synthesis method to other configurations are straightforward. Due to space limitation, they are omitted in this work.

VI. Conclusion

In this paper, a novel algorithm of accurate array response control (A^{2}RC) is devised. It is shown that the array pattern response at a given direction can be accurately adjusted to any predefined level. Besides, an effective mechanism of finding out a suitable weight vector which would not result in pattern distortion has been presented. The application of the A^{2}RC algorithm to pattern synthesis is then discussed. The proposed A^{2}RC based pattern synthesis approach successively control the responses at directions where deviations exist. In each step, it adjusts the response level at the given location by modifying the current weight vector with the help of a complex factor μ and the steering vector at the given direction. A number of examples under various problem settings have been carried out to demonstrate the effectiveness of the A^{2}RC approach. As a future work, we shall consider the problem of how to simultaneously control the pattern responses of multiple directions, so as to reduce the number of steps to achieve the desired pattern.

Appendix A
Proof of Proposition 1

For the sake of clarity, in the sequel, the real and imaginary parts of a complex number x are defined as

$$x_r = \mathrm{Re}(x), \;\; x_i = \mathrm{Im}(x). \tag{59}$$

For briefness, we consider the case that $\mathbb{D} = \mathbb{R}$. Then for any $\phi \in \mathbb{R}$, equation (34) can be alternatively represented by $(a_1 - cb_1)/(cb_2 - a_2) = e^{j\phi}$ and hence we have $|cb_1 - a_1| = |cb_2 - a_2|$. By applying the notations in (59), we get $|(c_r + jc_i)(b_{1r} + jb_{1i}) - (a_{1r} + ja_{1i})| = |(c_r + jc_i)(b_{2r} + jb_{2i}) - (a_{2r} + ja_{2i})|$, which can be written in a compact form as

$$f(\mathbf{c}) = \mathbf{c}^{\mathrm{T}}\mathbf{B}\mathbf{\Lambda}\mathbf{B}^{\mathrm{T}}\mathbf{c} - 2\mathbf{a}_\star^{\mathrm{T}}\mathbf{B}^{\mathrm{T}}\mathbf{c} + \mathbf{a}_1^{\mathrm{T}}\mathbf{a}_1 - \mathbf{a}_2^{\mathrm{T}}\mathbf{a}_2 = 0 \tag{60}$$

where $\mathbf{c} = [c_r \;\; c_i]^{\mathrm{T}}$, $\mathbf{\Lambda} = \mathrm{diag}\,([1 \;\; 1 \;\; -1 \;\; -1])$, $\mathbf{B} = [\mathbf{b}_1 \;\; \mathbf{P}\mathbf{b}_1 \;\; \mathbf{b}_2 \;\; \mathbf{P}\mathbf{b}_2]$, $\mathbf{b}_l = [b_{lr} \;\; -b_{li}]^{\mathrm{T}}$, $\mathbf{P} = \left[\begin{smallmatrix} & 1 \\ -1 & \end{smallmatrix}\right]$, $\mathbf{a}_\star = [\mathbf{a}_1^{\mathrm{T}} \;\; -\mathbf{a}_2^{\mathrm{T}}]^{\mathrm{T}}$, $\mathbf{a}_l = [a_{lr} \;\; a_{li}]^{\mathrm{T}} (l = 1, 2)$. A careful examination shows that $\mathbf{b}_l\mathbf{b}_l^{\mathrm{T}} + \mathbf{P}\mathbf{b}_l\mathbf{b}_l^{\mathrm{T}}\mathbf{P}^{\mathrm{T}} = \left(\mathbf{b}_l^{\mathrm{T}}\mathbf{b}_l\right)\mathbf{I}$ $(l = 1, 2)$ and $\mathbf{B}\mathbf{\Lambda}\mathbf{B}^{\mathrm{T}} = \left(\mathbf{b}_1^{\mathrm{T}}\mathbf{b}_1 - \mathbf{b}_2^{\mathrm{T}}\mathbf{b}_2\right)\mathbf{I}$. Let us define

$$h_a \triangleq \mathbf{a}_1^{\mathrm{T}}\mathbf{a}_1 - \mathbf{a}_2^{\mathrm{T}}\mathbf{a}_2, \; h_b \triangleq \mathbf{b}_1^{\mathrm{T}}\mathbf{b}_1 - \mathbf{b}_2^{\mathrm{T}}\mathbf{b}_2 \tag{61}$$

then $f(\mathbf{c})$ can be rewritten as

$$\begin{aligned} f(\mathbf{c}) &= h_b\mathbf{c}^{\mathrm{T}}\mathbf{c} - 2\mathbf{a}_\star^{\mathrm{T}}\mathbf{B}^{\mathrm{T}}\mathbf{c} + h_a \\ &= h_b\left(\mathbf{c} - \frac{1}{h_b}\mathbf{B}\mathbf{a}_\star\right)^{\mathrm{T}}\left(\mathbf{c} - \frac{1}{h_b}\mathbf{B}\mathbf{a}_\star\right) \\ &\quad - \frac{1}{h_b}\mathbf{a}_\star^{\mathrm{T}}\mathbf{B}^{\mathrm{T}}\mathbf{B}\mathbf{a}_\star + h_a = 0. \end{aligned} \tag{62}$$

This implies that $\mathbf{c}$ locates at a circle $\mathbb{C}_0$ with center of $\mathbf{c}_0 = \frac{1}{h_b}\mathbf{B}\mathbf{a}_\star$ and and a radius of

$$r_c = \sqrt{\frac{1}{h_b^2}\mathbf{a}_\star^{\mathrm{T}}\mathbf{B}^{\mathrm{T}}\mathbf{B}\mathbf{a}_\star - \frac{h_a}{h_b}}.$$

This completes the proof.

Appendix B
Proof of Proposition 2

Again, we use $x_r = \mathrm{Re}(x)$ and $x_i = \mathrm{Im}(x)$ to denote the real and imaginary parts of the complex number x, respectively. For simplicity, it is assumed that $\mathbb{F} = \mathbb{R}$ where $\mathbb{F}$ is defined as (33). From (32), we note that μ_k corresponds to c in (34) with $a_1 = u_{21}$, $a_2 = \sqrt{-\lambda_1/\lambda_2}u_{22}$, $b_1 = u_{11}$, $b_2 = \sqrt{-\lambda_1/\lambda_2}u_{12}$. According to Proposition 1, we have

$$\mathbf{a}_1 = \left[\begin{array}{cc} u_{21r} & u_{21i} \end{array}\right]^{\mathrm{T}} \tag{63}$$

$$\mathbf{a}_2 = \left[\begin{array}{cc} \sqrt{-\lambda_1/\lambda_2}u_{22r} & \sqrt{-\lambda_1/\lambda_2}u_{22i} \end{array}\right]^{\mathrm{T}} \tag{64}$$

$$\mathbf{b}_1 = \left[\begin{array}{cc} u_{11r} & -u_{11i} \end{array}\right]^{\mathrm{T}} \tag{65}$$

$$\mathbf{b}_2 = \left[\begin{array}{cc} \sqrt{-\lambda_1/\lambda_2}u_{12r} & -\sqrt{-\lambda_1/\lambda_2}u_{12i} \end{array}\right]^{\mathrm{T}} \tag{66}$$

$$\mathbf{a}_\star = \left[\begin{array}{cccc} u_{21r} & u_{21i} & -\sqrt{-\frac{\lambda_1}{\lambda_2}}u_{22r} & -\sqrt{-\frac{\lambda_1}{\lambda_2}}u_{22i} \end{array}\right]^{\mathrm{T}} \tag{67}$$

$$\mathbf{B} = \left[\begin{array}{cccc} u_{11r} & u_{11i} & \sqrt{-\frac{\lambda_1}{\lambda_2}}u_{12r} & \sqrt{-\frac{\lambda_1}{\lambda_2}}u_{12i} \\ -u_{11i} & u_{11r} & -\sqrt{-\frac{\lambda_1}{\lambda_2}}u_{12i} & \sqrt{-\frac{\lambda_1}{\lambda_2}}u_{12r} \end{array}\right] \tag{68}$$

Recalling (61), we have

$$h_a = |u_{21}|^2 + (\lambda_1/\lambda_2)|u_{22}|^2 \tag{69}$$

$$h_b = |u_{11}|^2 + (\lambda_1/\lambda_2)|u_{12}|^2. \tag{70}$$

Let us first derive the coordinate of $\mathbf{c}_\mu$, which represents the center of the distribution circle. From (35), $\mathbf{c}_\mu$ can be described as

$$\mathbf{c}_\mu = \frac{1}{h_b}\mathbf{B}\mathbf{a}_\star = \frac{\left[\begin{array}{c} (u_{11r}u_{21r} + u_{11i}u_{21i})(\lambda_2 - \lambda_1) \\ (u_{11r}u_{21i} - u_{11i}u_{21r})(\lambda_2 - \lambda_1) \end{array}\right]}{\lambda_2|u_{11}|^2 + \lambda_1|u_{12}|^2}. \tag{71}$$

It should be noted that in the above equation, the orthogonality of row vectors of $\mathbf{U}$ has been utilized, i.e., $\left[\begin{array}{cc} u_{11}^* & u_{12}^* \end{array}\right]\left[\begin{array}{cc} u_{21} & u_{22} \end{array}\right]^{\mathrm{T}} = 0$, which can be also written as

$$(u_{11r}u_{21r} + u_{11i}u_{21i}) + (u_{12r}u_{22r} + u_{12i}u_{22i}) = 0 \tag{72}$$

$$(u_{11r}u_{21i} - u_{11i}u_{21r}) + (u_{12r}u_{22i} - u_{12i}u_{22r}) = 0. \tag{73}$$

Since $\mathbf{Q} = \mathbf{U}\mathbf{\Lambda}\mathbf{U}^{\mathrm{H}}$, according to (72) and (73), we have

$$\mathrm{Re}(\mathbf{Q}(1,2)) = (\lambda_1 - \lambda_2)(u_{11r}u_{21r} + u_{11i}u_{21i}) \tag{74}$$

$$\mathrm{Im}(\mathbf{Q}(1,2)) = (\lambda_2 - \lambda_1)(u_{11r}u_{21i} - u_{11i}u_{21r}). \tag{75}$$

As a result, the numerator of the last term of (71) can be written as $[-\mathrm{Re}(\mathbf{Q}(1,2)) \;\; \mathrm{Im}(\mathbf{Q}(1,2))]^{\mathrm{T}}$.

We now proceed to consider the denominator of $\mathbf{c}_\mu$ in the last term of (71). By expanding $\mathbf{Q} = \mathbf{U}\mathbf{\Lambda}\mathbf{U}^{\mathrm{H}}$, it can be readily obtained that

$$\lambda_1|u_{21}|^2 + \lambda_2|u_{22}|^2 = \mathbf{Q}(2,2). \tag{76}$$

Since $\mathbf{U}$ is an unitary matrix, we have $|u_{11}|^2 + |u_{12}|^2 = |u_{12}|^2 + |u_{22}|^2 = |u_{11}|^2 + |u_{21}|^2 = 1$, which further yields

$$|u_{12}|^2 = |u_{21}|^2,\ |u_{11}|^2 = |u_{22}|^2. \tag{77}$$

Then, by combining (76) and (77), one gets

$$\lambda_2|u_{11}|^2 + \lambda_1|u_{12}|^2 = \mathbf{Q}(2,2). \tag{78}$$

Consequently, it can be concluded that

$$\mathbf{c}_\mu = \frac{\begin{bmatrix} -\mathrm{Re}(\mathbf{Q}(1,2)) \\ \mathrm{Im}(\mathbf{Q}(1,2)) \end{bmatrix}}{\mathbf{Q}(2,2)}. \tag{79}$$

Now, we move to the discussion of r_μ. From (71), we get

$$\mathbf{a}_\star^{\mathrm{T}}\mathbf{B}^{\mathrm{T}}\mathbf{B}\mathbf{a}_\star = (1-\lambda_1/\lambda_2)^2\,|u_{11}|^2|u_{21}|^2. \tag{80}$$

Combining (69), (70), (77), and (80), the following compact expression is obtained

$$\mathbf{a}_\star^{\mathrm{T}}\mathbf{B}^{\mathrm{T}}\mathbf{B}\mathbf{a}_\star - h_a h_b = -\lambda_1/\lambda_2. \tag{81}$$

Since $\det(\mathbf{Q}) = \lambda_1\lambda_2$, r_μ^2 can be obtained from (78) and (81)

$$r_\mu^2 = \frac{\mathbf{a}_\star^{\mathrm{T}}\mathbf{B}^{\mathrm{T}}\mathbf{B}\mathbf{a}_\star - h_a h_b}{h_b^2} = \frac{-\det(\mathbf{Q})}{\mathbf{Q}^2(2,2)} \tag{82}$$

which can be reexpressed as

$$r_\mu = \frac{\sqrt{-\det(\mathbf{Q})}}{|\mathbf{Q}(2,2)|}. \tag{83}$$

This completes the proof.

ACKNOWLEDGMENT

The authors would like to thank the anonymous reviewers for their valuable comments and suggestions.

REFERENCES

[1] R. J. Mailous, *Phased Array Antenna Handbook*. Norwood, MA, USA: Artech House, 1994.
[2] K. M. Tsui and S. C. Chan, "Pattern synthesis of narrowband conformal arrays using iterative second-order cone programming," *IEEE Trans. Antennas Propag.*, vol. 58, no. 6, pp. 1959–1970, Jun. 2010.
[3] M. H. Er, "Array pattern synthesis with a controlled mean-square sidelobe level," *IEEE Trans. Signal Process.*, vol. 40, no. 4, pp. 977–981, Apr. 1992.
[4] B. Fuchs and J. J. Fuchs, "Optimal narrow beam low sidelobe synthesis for arbitrary arrays," *IEEE Trans. Antennas Propag.*, vol. 58, no. 6, pp. 2130–2135, Jun. 2010.
[5] C. L. Dolph, "A current distribution for broadside arrays which optimizes the relationship between beam width and side-lobe level," *Proc. IRE*, vol. 34, no. 6, pp. 335–348, Jun. 1946.
[6] K. Chen, X. Yun, Z. He, and C. Han, "Synthesis of sparse planar arrays using modified real genetic algorithm," *IEEE Trans. Antennas Propag.*, vol. 55, no. 4, pp. 1067–1073, Apr. 2007.
[7] D. W. Boeringer and D. H. Werner, "Particle swarm optimization versus genetic algorithms for phased array synthesis," *IEEE Trans. Antennas Propag.*, vol. 52, no. 3, pp. 771–779, Mar. 2004.
[8] V. Murino, A. Trucco, and C. S. Regazzoni, "Synthesis of unequally spaced arrays by simulated annealing," *IEEE Trans. Signal Process.*, vol. 44, no. 1, pp. 119–122, Jan. 1996.
[9] H. K. Van Trees, *Optimum Array Processing*. New York, NY, USA: Wiley, 2002.
[10] J. Li and P. Stoica Eds., *Robust Adaptive Beamforming*. Hoboken, NJ, USA: Wiley, 2005.
[11] I. S. Reed, J. D. Mallett, and L. E. Brennan, "Rapid convergence rate in adaptive arrays," *IEEE Trans. Aerosp. Electron. Syst.*, vol. AES-10, no. 6, pp. 853–863, Nov. 1974.
[12] C. Y. Tseng and L. J. Griffiths, "A simple algorithm to achieve desired patterns for arbitrary arrays," *IEEE Trans. Signal Process.*, vol. 40, no. 11, pp. 2737–2746, Nov. 1992.
[13] C. A. Olen and R. T. Compton, "A numerical pattern synthesis algorithm for arrays," *IEEE Trans. Antennas Propag.*, vol. 38, no. 10, pp. 1666–1676, Oct. 1990.
[14] P. Y. Zhou and M. A. Ingram, "Pattern synthesis for arbitrary arrays using an adaptive array method," *IEEE Trans. Antennas Propag.*, vol. 47, no. 5, pp. 862–869, May 1999.
[15] W. A. Swart and J. C. Olivier, "Numerical synthesis of arbitrary discrete arrays," *IEEE Trans. Antennas Propag.*, vol. 41, no. 8, pp. 1171–1174, Aug. 1993.
[16] P. Y. Zhou, M. A. Ingram, and P. D. Anderson, "Synthesis of minimax sidelobes for arbitrary arrays," *IEEE Trans. Antennas Propag.*, vol. 46, no. 11, pp. 1759–1760, Nov. 1998.
[17] H. Lebret and S. Boyd, "Antenna array pattern synthesis via convex optimization," *IEEE Trans. Signal Process.*, vol. 45, no. 3, pp. 526–532, Mar. 1997.
[18] W. Fan, V. Balakrishnan, P. Y. Zhou, J. J. Chen, R. Yang, and C. Frank, "Optimal array pattern synthesis using semidefinite programming," *IEEE Trans. Signal Process.*, vol. 51, no. 5, pp. 1172–1183, May 2003.
[19] B. Fuchs, "Application of convex relaxation to array synthesis problems," *IEEE Trans. Antennas Propag.*, vol. 62, no. 2, pp. 634–640, Feb. 2014.
[20] P. Rocca, G. Oliveri, R. J. Mailloux, and A. Massa, "Unconventional phased array architectures and design methodologies—A review," *Proc. IEEE*, vol. 104, no. 3, pp. 544–560, Mar. 2016.

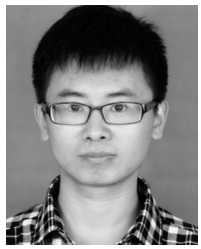

Xuejing Zhang (S'17) was born in Hebei, China. He received the B.S. degree in electrical engineering from Huaqiao University, Xiamen, China and the M.S. degree in signal and information processing from Xidian University, Xi'an, China, in 2011 and 2014, respectively. He is currently working toward the Ph.D. degree in signal and information processing at the Department of Electronic Engineering, University of Electronic Science and Technology of China, Chengdu, China. From 2014 to 2015, he was a Research Engineer in Allwinner, Inc., Zhuhai, China, where he was engaged in algorithmic research. His research interests include array signal processing, optimization theory, and machine learning.

Zishu He (M'11) was born in Chengdu, China, in 1962. He received the B.S., M.S., and Ph.D. degrees in signal and information processing from the University of Electronic Science and Technology of China (UESTC), Chengdu, China, in 1984, 1988, and 2000, respectively.

He is currently a Professor of signal and information processing in the School of Electronic Engineering, UESTC. His research interests include array signal processing, digital beam forming, the theory on MIMO communication and MIMO radar, adaptive signal processing, and interference cancellation.

Bin Liao (S'09–M'13–SM'16) received the B.Eng. and M.Eng degrees from Xidian University, Xian, China, and the Ph.D. degree from The University of Hong Kong, Hong Kong, in 2006, 2009, and 2013, respectively. From September 2013 to January 2014, he was a Research Assistant in the Department of Electrical and Electronic Engineering, The University of Hong Kong. From August 2016 to October 2016, he was a Research Scientist in the Department of Electrical and Electronic Engineering, The University of Hong Kong. He is currently an Associate Professor in the College of Information Engineering, Shenzhen University, Shenzhen, China. His research interests include sensor array processing, adaptive filtering, convex optimization, with applications to radar, navigation, and communications.

Dr. Liao is an Associate Editor of *Multidimensional Systems and Signal Processing* and IEEE ACCESS. He received the 2016 IEEE DSP Best Paper Award.

Xuepan Zhang was born in Hebei, China. He received the B.S. and Ph.D. degrees from the National Laboratory of Radar Signal Processing, Xidian University, Xi'an, China, in 2010 and 2015, respectively, both in electrical engineering. He is currently a Principal Investigator in Qian Xuesen Laboratory of Space Technology, Beijing, China. His research interests include synthetic aperture radar, ground moving target indication, and machine learning.

Ziyang Cheng is currently working toward the Ph.D. degree in signal and information processing at the University of Electronic Science and Technology of China, Chengdu, China. His research interests include MIMO radar waveform design and radar target detection.

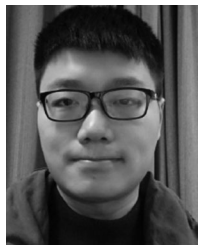

Yanxi Lu (S'14) received the B.Eng. degree in electronic engineering, in 2013, from the University of Electronic Science and Technology of China (UESTC), Chengdu, China, where he is currently working toward the Ph.D degree in electronic engineering. His research interests include statistical signal processing, wireless sensor network, and MIMO radar.